Transthyretin Aggregation under Partially Denaturing Conditions Is a Downhill Polymerization†

Amy R. Hurshman, Joleen T. White, Evan T. Powers, and Jeffery W. Kelly*

Department of Chemistry and Skaggs Institute for Chemical Biology, The Scripps Research Institute, 10550 North Torrey Pines Road BCC-506, La Jolla, California 92037

Received February 21, 2004; Revised Manuscript Received April 5, 2004

ABSTRACT: The deposition of fibrils and amorphous aggregates of transthyretin (TTR) in patient tissues is a hallmark of TTR amyloid disease, but the molecular details of amyloidogenesis are poorly understood. Tetramer dissociation is typically rate-limiting for TTR amyloid fibril formation, so we have used a monomeric variant of TTR (M-TTR) to study the mechanism of aggregation. Amyloid formation is often considered to be a nucleation-dependent process, where fibril growth requires the formation of an oligomeric nucleus that is the highest energy species on the pathway. According to this model, the rate of fibril formation should be accelerated by the addition of preformed aggregates or "seeds", which effectively bypasses the nucleation step. Herein, we demonstrate that M-TTR amyloidogenesis at low pH is a complex, multistep reaction whose kinetic behavior is incompatible with the expectations for a nucleation-dependent polymerization. M-TTR aggregation is not accelerated by seeding, and the dependence of the reaction timecourse is first-order on the M-TTR concentration, consistent either with a dimeric nucleus or with a nonnucleated process where each step is bimolecular and essentially irreversible. These studies suggest that amyloid formation by M-TTR under partially denaturing conditions is a downhill polymerization, in which the highest energy species is the native monomer. Our results emphasize the importance of therapeutic strategies that stabilize the TTR tetramer and may help to explain why more than eighty TTR variants are disease-associated. The differences between amyloid formation by M-TTR and other amyloidogenic peptides (such as amyloid β-peptide and islet amyloid polypeptide) demonstrate that these polypeptides do not share a common aggregation mechanism, at least under the conditions examined thus far.

A number of human diseases are characterized by protein deposition in the form of highly ordered structures known as amyloid fibrils (*1*−*4*). The most familiar and clinically important of the amyloid diseases is Alzheimer's disease, associated with the aggregation of the amyloid β-peptide (Aβ)[1] in the brain of affected individuals (*5*). Amyloid fibrils have been implicated in the etiology of several other diseases as well, including type II diabetes, light chain amyloidosis, and familial amyloid polyneuropathy (FAP) (*1*−*4*). The presence of amyloid fibrils is a hallmark of all amyloid diseases, leading to the hypothesis that either the accumulation of fibrils or the process of fibril formation is responsible for disease pathology and progression (*6*, *7*). Although the identity of the polypeptide involved in fibril formation and deposition is disease-specific, comparison of the amyloid fibrils formed in each case suggests a common morphology and a similar cross-β-sheet quaternary structure (*8*), as evaluated by X-ray fibril diffraction, electron and atomic force microscopy, and the binding of amyloid-selective dyes such as Congo red and thioflavin T (TfT). This common amyloid structure is formed despite an apparent lack of homology in sequence, native structure, or function among the various amyloidogenic proteins and peptides (*9*).

Although there is genetic and biochemical evidence supporting the so-called amyloid hypothesis, namely that amyloid fibril formation is responsible for the development of disease, it is not clear exactly how abnormal protein aggregation leads to cellular dysfunction nor which structural species may be involved in the pathology of amyloid disease. Several recent studies have demonstrated that the severity and localization of disease in patients with Alzheimer's disease and FAP correlate better with the presence of soluble aggregates than with the presence of mature amyloid fibrils (*10*−*12*). Additional studies in mammalian tissue culture and in animal model systems show that small aggregates in the fibril formation pathway appear to be considerably more toxic than mature fibrils for several amyloidogenic proteins (*13*−*19*). Taken together, these data suggest that early oligomeric intermediates have significant toxicity that may be relevant to disease pathology (*20*). A thorough under-

† This research was supported by NIH Grant DK46335, the Skaggs Institute for Chemical Biology, and the Lita Annenberg Hazen Foundation. A. R. H. was supported by NIH Grants T32-AG00080 and F32-GM067348. J. T. W. was supported by the National Science Foundation and the William and Sharon Bauce Foundation.

* To whom correspondence should be addressed. Phone: (858) 784−9601. Fax: (858) 784−9610. E-mail: jkelly@scripps.edu.

[1] Abbreviations: Aβ, amyloid β-peptide; TTR, transthyretin; wtTTR, wild-type transthyretin; M-TTR, a monomeric form of transthyretin, engineered by F87M/L110M mutations; SSA, senile systemic amyloidosis; FAP, familial amyloid polyneuropathy; FAC, familial amyloid cardiomyopathy; IAPP, islet amyloid polypeptide; IPTG, isopropyl-β-D-thiogalactopyranoside; Tris, Tris(hydroxymethyl)aminomethane; PMSF, phenylmethylsulfonyl fluoride; EDTA, ethylenediamine-*N*,*N*,*N*′,*N*′-tetraacetic acid; TfT, thioflavin T; AFM, atomic force microscopy; EM, electron microscopy; SDS−PAGE; sodium dodecyl sulfate-polyacrylamide gel electrophoresis; *n**, nucleus size.

10.1021/bi049621l CCC: $27.50
Published on Web 05/14/2004

standing of the pathway and mechanism of amyloidogenesis is important for the development of useful therapeutic strategies for these diseases (*21*).

In this paper, we have investigated the aggregation mechanism of transthyretin (TTR), a 55-kDa homotetramer composed of 127-amino acid, β-sheet rich subunits (*22*, *23*). TTR is normally present in human plasma (physiological concentration of 0.1−0.4 mg/mL), where it functions in the binding and transport of thyroid hormone (thyroxine, T_4) and the retinol binding protein/vitamin A complex (*24*). TTR is also present at lower concentrations (∼0.02 mg/mL) and is the primary carrier of thyroxine in cerebrospinal fluid. TTR amyloid fibril formation is associated with the development of several diseases. Senile systemic amyloidosis (SSA) occurs after age 60 and is characterized by deposition of wild-type TTR (wtTTR) (*25*, *26*). This disease is usually mild but can lead to congestive heart failure and may affect as much as 25% of the population over 80 years of age. More than 80 point mutations in TTR have been described and are implicated in autosomal dominant disorders known either as familial amyloid polyneuropathy (FAP) or familial amyloid cardiomyopathy (FAC), depending on the primary site(s) of amyloid deposition (*27*−*29*). FAP and FAC are characterized by an early age of onset, as early as the second decade for the most severe mutations, and typically demonstrate a more aggressive pathology than SSA. Amyloid fibrils isolated from heterozygous patients with these familial diseases are composed primarily of variant TTR (*27*), suggesting that mutations in TTR increase its amyloidogenicity in vivo.

Most of the FAP/FAC mutations are conservative, resulting in little or no perturbation to the overall structure of the folded tetramer, as determined by crystallographic studies (*30*−*32*). A number of these mutations (e.g., L55P, V30M, and V122I) do influence the thermodynamic stability and the kinetics of dissociation of the TTR tetramer in vitro, and these properties of the variant tetramers appear to be correlated to the severity of the resulting disease (*33*−*40*). There are also suppressor mutations in TTR (e.g., T119M) that kinetically stabilize the native tetramer (*38*, *41*−*43*) and are protective against the development of FAP/FAC in compound heterozygotes carrying a disease-associated mutation (*44*, *45*). Previous studies have shown that tetramer dissociation is the rate-limiting step for amyloidogenesis in vitro (*46*, *47*), providing a potential explanation for the observed correlation between the kinetic and thermodynamic stability of TTR tetramers and their amyloidogenicity (*40*). However, tetramer dissociation is not sufficient to initiate fibril formation, since native monomers of wtTTR are not aggregation-competent. Partial denaturation is also required to form the amyloidogenic intermediate (*46*−*50*), which is proposed to be a partially unfolded monomeric species (*51*), suggesting that differences in tertiary structure stability may also influence the pathogenicity of various TTR mutants (*50*).

The details of TTR fibril formation from the monomeric amyloidogenic intermediate are not well understood. Hypotheses concerning the mechanism of amyloid fibril formation are derived primarily from results obtained with Aβ (*52*−*55*), where the observed kinetics of amyloidogenesis suggest a nucleation-dependent polymerization process much like that which characterizes crystal growth (Scheme 1A). In this model, aggregation requires the formation of a thermodynamic nucleus (*56*−*60*), composed of n^* monomers, which is defined as the highest energy species along the reaction pathway. Hence, nucleation is rate-limiting for amyloidogenesis; the rate of aggregation is expected to have a high-order dependence (where the order is related to n^*) on the concentration of protein or peptide monomer. Furthermore, fibril formation should be accelerated by the addition of preformed aggregates or "seeds", which effectively bypasses the rate-limiting nucleation step. Fibril formation by wild-type tetrameric TTR is not seedable (*46*); however, this lack of seeding is expected, because the rate-limiting step in TTR aggregation is tetramer dissociation rather than nucleation (Scheme 1B)

To facilitate the elucidation of the aggregation pathway, we have chosen to use a monomeric TTR variant (M-TTR) developed in our laboratory (*47*). M-TTR was designed by introducing two methionine mutations (F87M and L110M) that disrupt the subunit interfaces of the TTR tetramer. Biophysical characterization of M-TTR shows it to be nearly exclusively (>95%) monomeric at physiological concentrations and to have very similar tertiary structure and tertiary structural stability to native monomeric wtTTR (*47*). M-TTR aggregates readily only under partially denaturing conditions, confirming that the native monomer is not amyloidogenic and that partial unfolding of the monomer is required for amyloid formation. Although both M-TTR and tetrameric wtTTR are susceptible to aggregation under similar conditions, the rate of M-TTR aggregation is ∼100-fold faster than that of wtTTR (*47*). Since the tertiary structural stabilities of M-TTR and wtTTR monomers are similar, this observation is consistent with rate-limiting tetramer dissociation. The advantage to using M-TTR in the studies reported here is that it allows separation of the kinetics of amyloidogenesis from those of tetramer dissociation. Furthermore, the dependence of aggregation on a variety of environmental conditions (e.g., pH, temperature, ionic strength, protein concentration) can be examined without having to account for the potential effect of these variables on the tetramer−monomer equilibrium.

In this work, we have used a variety of techniques to study the aggregation of M-TTR and to test whether this process is a nucleation-dependent polymerization (Scheme 1B) similar to that described for amyloidogenic peptides such as Aβ and islet amyloid polypeptide (IAPP; Scheme 1A). We show that M-TTR amyloidogenesis is a complex, multistep reaction whose kinetic behavior is not compatible with the expectations for a nucleated process. The aggregation of M-TTR does not show a high-order dependence on the concentration of monomeric protein and is not accelerated by seeding, suggesting that it does not require the formation of a high-energy oligomeric nucleus. These studies have important implications for understanding the progression of TTR amyloid disease and for developing effective therapeutic strategies for the treatment of these disorders.

EXPERIMENTAL PROCEDURES

Expression and Purification of M-TTR. M-TTR was expressed in BL21(DE3) Epicurian Gold cells (Stratagene, La Jolla, CA) transformed with the M-TTR/pMMHa expression vector (*47*). A starter culture (in LB with 100 μg/mL ampicillin) was grown at 37 °C until cell growth was visible.

Scheme 1: Model for Nucleation-Dependent Polymerization[a]

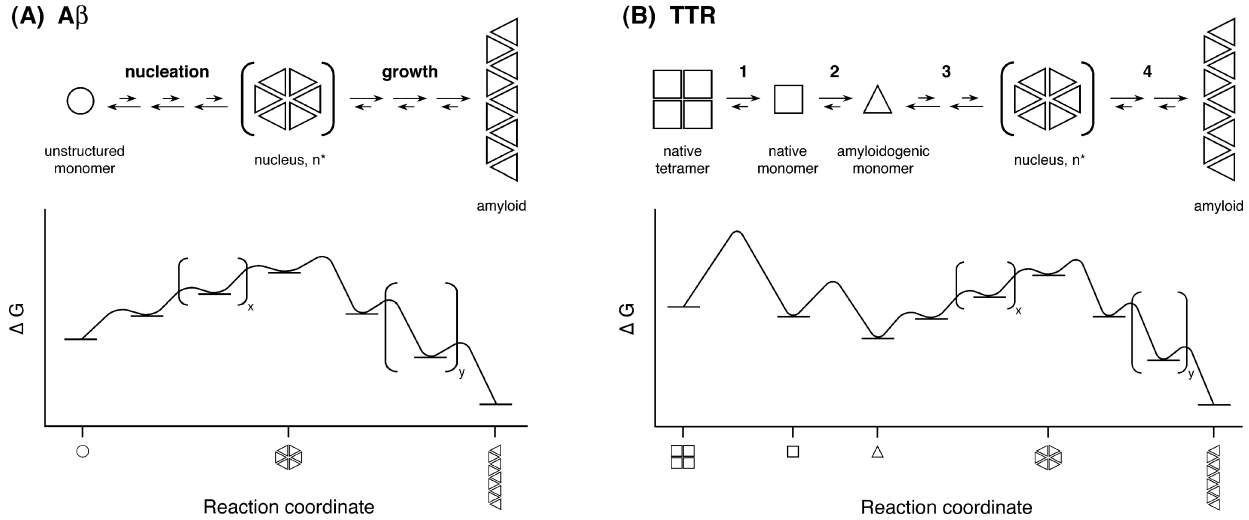

[a] The classical model for nucleation-dependent polymerization is shown for (**A**) Aβ peptide and (**B**) as modified for TTR amyloidogenesis. (**A**) Amyloid formation from monomeric proteins and peptides is proposed to proceed by a mechanism similar to crystallization. In this model, the assembly of protein into amyloid fibrils is characterized by two phases—nucleation and growth. The initial steps of aggregation involve the formation of the nucleus and are described by a series of unfavorable equilibria (nucleation phase). Once an oligomeric nucleus has formed, the subsequent addition of monomers to the growing polymer becomes energetically favorable (growth phase). The main feature of this model is the existence of a thermodynamic nucleus as the key intermediate in the aggregation pathway. The nucleus consists of *n** peptide or protein subunits and is the highest energy species along the pathway, as illustrated by the free-energy diagram. The number of individual steps in the nucleation and growth phases is not specified in this model, as indicated by the repeating units *x* and *y*, respectively. The rate of nucleation-dependent polymerization reactions show a high-order dependence on the concentration of monomeric protein or peptide and can be dramatically increased by "seeding", the addition of preformed fibrils. (**B**) The model for nucleation-dependent polymerization has been adapted for TTR amyloidogenesis, to account for the fact that TTR is a natively folded, tetrameric protein rather than an unstructured monomeric peptide like Aβ. Previous studies have shown that dissociation of the TTR tetramer (step **1**) is the rate-limiting step for fibril formation in vitro. Furthermore, the resulting monomer only becomes amyloidogenic when subjected to partially denaturing conditions, suggesting that a structural rearrangement of the monomer (step **2**) is also required. The subsequent aggregation process is identical to that shown for Aβ, involving both a nucleation phase (step **3**) and a growth phase (step **4**). The partially denaturing conditions required for TTR amyloidogenesis change the free-energy landscape from that which exists under native conditions, where the TTR tetramer is more stable than either TTR monomeric species.

Expression cultures (1.5 L of LB containing 100 μg/mL ampicillin) were inoculated at 1:100 dilution from the starter culture and were grown at 37 °C to an A_{600} of ~1. The cultures were induced by the addition of IPTG (1 mM final concentration), grown overnight at 37 °C, and harvested by centrifugation (10 min at 13 700*g*). Fresh cell pellets were resuspended in 20 mM Tris, 500 mM NaCl (pH 7.5; 100 mL buffer/L of culture) and were frozen in aliquots at −80 °C. Resuspended cells (one 200-mL aliquot for a typical purification) were thawed in a 37 °C water bath, lysed by sonication (3 × 3-min cycles, with 6-s pulses) in the presence of protease inhibitors (8 μg/mL benzamidine, 5 μg/mL *o*-phenanthroline, and 0.5 mM PMSF), and centrifuged for 30 min at 24 300*g*. The supernatant was fractionated with ammonium sulfate; the 25−100% ammonium sulfate pellet was resuspended in a minimal volume of 25 mM Tris, 1 mM EDTA (pH 8.0) and was dialyzed in 3500 MWCO dialysis tubing (Snakeskin from Pierce Biotechnology, Rockford, IL) against 4 L of 25 mM Tris, 1 mM EDTA (pH 8.0) overnight at 4 °C. After dialysis, the sample was filtered and applied to a Source 15Q anion exchange column (Amersham Biosciences, Piscataway, NJ) equilibrated with 25 mM Tris, 1 mM EDTA, 50 mM NaCl (pH 8.0). M-TTR was eluted with a linear gradient of 50−350 mM NaCl in 1.5 column volumes followed by a 350 mM NaCl wash for 1.5 column volumes. Fractions containing M-TTR (the major peak) were pooled, concentrated, and further purified on a Superdex 75 gel filtration column (Amersham Biosciences, Piscataway, NJ) in 10 mM sodium phosphate, 100 mM KCl, and 1 mM EDTA (pH 7.0) to remove any soluble aggregates. Concentrations of M-TTR solutions are expressed in mg/mL and were determined spectrophotometrically, using an ϵ_{280} of 1.35 $(mg/mL)^{-1}$ cm^{-1}. A typical purification, as described here, yields 40−60 mg of M-TTR from 2 L of cell culture; the M-TTR thus obtained is >95% monomeric, as previously reported (*47*). M-TTR solutions were stored at 4 °C and were used within a week of purification.

Aggregation Kinetics. Reactions were initiated by the addition of M-TTR stock solutions (0.1−0.8 mg/mL) in 10 mM sodium phosphate, 100 mM KCl, and 1 mM EDTA (pH 7.0) to an equivalent volume of 200 mM sodium acetate, 100 mM KCl, and 1 mM EDTA (pH 4.3), and aggregation was assessed by several methods. All reactions were carried out at 37 °C; both solutions (M-TTR stocks and the acetate buffer) were equilibrated to 37 °C before mixing.

(*A*) *Turbidity Measurements.* Assays (total volume 1 mL) contained 0.05−0.4 mg/mL M-TTR, 100 mM KCl, and 1 mM EDTA in 5 mM sodium phosphate and 100 mM sodium acetate buffers at pH 4.4 and were carried out at 37 °C with no stirring. The increase in turbidity at 400 nm throughout the reaction was measured on an HP 8453 UV−vis spectrophotometer (Agilent Technologies, Palo Alto, California), equipped with a Peltier temperature controller. Data were collected at 10-s intervals until a total time of 3600 s (1 h), except for the lowest M-TTR concentrations (0.05 and 0.1 mg/mL), where data were collected for 7200 s (2 h).

(*B*) *Thioflavin T Binding.* Reactions were initiated as described above, except that TfT (50 μL of a 2 mM stock solution in 10 mM sodium phosphate, 100 mM KCl, and

1 mM EDTA, pH 7.0) was added to the acetate buffer prior to the addition of M-TTR. Assays (total volume 2.05 mL) contained 0.05−0.4 mg/mL M-TTR, 100 mM KCl, 1 mM EDTA, and 48.8 μM TfT in 5.1 mM sodium phosphate and 97.6 mM sodium acetate buffers at pH 4.4 and were carried out at 37 °C with no stirring. TfT fluorescence was monitored continuously, using an AVIV ATF-105 fluorometer (AVIV Instruments, Lakewood, NJ) with 440 nm excitation (1.5 nm bandwidth) and 485 nm emission (6 nm bandwidth). Data were collected at 5-s intervals until a total time of 1800 s (30 min). For each experiment, control TfT reactions were carried out either at pH 4.4 with no M-TTR (48.8 μM TfT, 100 mM KCl, and 1 mM EDTA in 5.1 mM sodium phosphate and 97.6 mM sodium acetate buffers) or at pH 7.0 with varying M-TTR concentrations (0.05−0.4 mg/mL, with 48.8 μM TfT, 100 mM KCl, and 1 mM EDTA in 10 mM sodium phosphate). Kinetic traces for each M-TTR concentration were corrected by subtracting either the corresponding pH 7.0 control reaction or the pH 4.4 control.

For some control experiments, aggregation reactions were carried out in the absence of TfT and were assayed for TfT binding at various times throughout the reaction. These reactions contained 0.05−0.4 mg/mL M-TTR, 100 mM KCl, and 1 mM EDTA in 5 mM sodium phosphate and 100 mM sodium acetate buffers at pH 4.4 and were carried out in microcentrifuge tubes at 37 °C with no stirring. Reactions were vortexed prior to removal of aliquots, and TfT measurements were made at pH 4.4 by adding 50 μM TfT to each aliquot immediately prior to recording the fluorescence emission spectrum.

(*C*) *Analytical Gel Filtration.* Assays (300 μL total volume) were carried out in microcentrifuge tubes and were incubated for the desired length of time (30−7200 s) at 37 °C with no stirring. After incubation, reaction mixtures (100-μL injections) were analyzed by gel filtration on a Superdex 75 HR 10/30 column (10 × 300 mm, 13 μm, from Amersham Biosciences, Piscataway, NJ) at 25 °C, with detection at 280 nm. The mobile phase was 10 mM sodium phosphate buffer containing 100 mM KCl and 1 mM EDTA (pH 7.0). At longer time points, where large aggregates were present, reaction mixtures were centrifuged at 16 000*g* for 5 min at 4 °C prior to injection on the column. Samples incubated for short times were not centrifuged; control experiments showed that the chromatograms for these samples were identical whether they were centrifuged or not. Concentrations of each peak were calculated from a standard curve of varying concentrations of M-TTR stock solutions (0.001−0.8 mg/mL) prepared in 10 mM sodium phosphate with 100 mM KCl and 1 mM EDTA (pH 7.0).

Determination of Nucleus Size and Critical Concentration for Aggregation. (*A*) *Nucleus Size*. Kinetic traces from the turbidity and TfT fluorescence assays were analyzed. For each trace, the endpoint amplitude was measured, and the time required to reach half-maximal amplitude (defined as t_{50}) was calculated. The nucleus size can be extracted from the dependence of the rate of reaction on the concentration of M-TTR (*59*), calculated as the slope of ln t_{50} vs ln [M-TTR].

(*B*) *Critical Concentration.* Aggregation reactions (0.01−0.4 mg/mL M-TTR) were carried out in microcentrifuge tubes with no stirring. At various times (1, 24, and 48 h), the reactions were vortexed to ensure that the mixtures were homogeneous, and aliquots were removed for turbidity and TfT measurements. For turbidity assays, samples containing a large amount of aggregated protein (turbidity >1 at 400 nm) were diluted to obtain turbidity values within the linear range of the instrument and to accurately determine the endpoint. TfT measurements were made at pH 4.4 by adding 50 μM TfT to each aliquot immediately prior to recording the fluorescence emission spectrum. The endpoint turbidity and TfT fluorescence were thus determined for each M-TTR concentration; the critical concentration for aggregation can be estimated from the *x*-intercept of the plot of endpoint amplitudes versus concentration of M-TTR (*58*).

The critical concentration for aggregation was also determined from the equilibrium concentration of monomer in aggregating reactions. Concentrations of monomer were measured by gel filtration (vide supra) at long reaction times (3 h to 1 wk). Samples were centrifuged at 16 000*g* for 5 min at 4 °C to remove large aggregates prior to analysis.

Seeding Experiments. M-TTR aggregation reactions that had proceeded for varying lengths of time (1 min to 3 days) at pH 4.4 and 37 °C were evaluated for their ability to seed the aggregation of fresh M-TTR. These seeded reactions were carried out exactly as described above, except that seed mixtures were added to the low pH acetate buffer immediately prior to the addition of M-TTR. Seeds were either vortexed for 5 s or sonicated for 2 min and then vortexed, to ensure that a homogeneous mixture was being used. The total concentration of M-TTR was identical to that in unseeded reactions, but 2, 5, or 10% (w/w) of the total M-TTR present in the final assay came from the seed mixtures. The final pH of the seeded reactions and final concentrations for all assay components were identical to those used in the unseeded reactions. For example, a reaction of 0.2 mg/mL M-TTR with 10% seed was carried out as follows: (1) 0.2 mg/mL M-TTR seed (300 μL total volume) was prepared by incubation at pH 4.4 and 37 °C for the desired length of time, and (2) the seeded reaction was initiated by addition of 200 μL of seed and 900 μL of fresh M-TTR (0.4 mg/mL) to a cuvette containing 900 μL of acetate buffer. Aggregation was monitored both by turbidity and TfT fluorescence.

Microscopy. Aliquots were removed from M-TTR aggregation reactions at varying time points (60−3600 s), and the aggregates were examined by AFM and EM. All microscopy samples were derived from reactions of 0.2 mg/mL M-TTR carried out at pH 4.4 and 37 °C.

(*A*) *Atomic Force Microscopy.* For each time point, an aliquot (20 μL) of the reaction solution was placed on a 0.8- × 0.8-cm piece of freshly cleaved mica and was allowed to adsorb to the mica surface for 10 s. The excess solution was wicked away with filter paper, and the mica surface was washed three times with deionized water. Following the final water wash, the excess water was carefully removed with filter paper, and the sample was air-dried overnight. A solution of 0.2 mg/mL M-TTR in 10 mM sodium phosphate, 100 mM KCl, and 1 mM EDTA (pH 7.0), prepared in exactly the same manner, was used as a $t = 0$ control. AFM images in height and amplitude mode were obtained in air, using a Digital Instruments Multimode scanning probe microscope with a Nanoscope IIIa controller (Digital Instruments, Santa Barbara, CA) operating in tapping mode with force-modulation etched silicon probes (Digital Instruments model

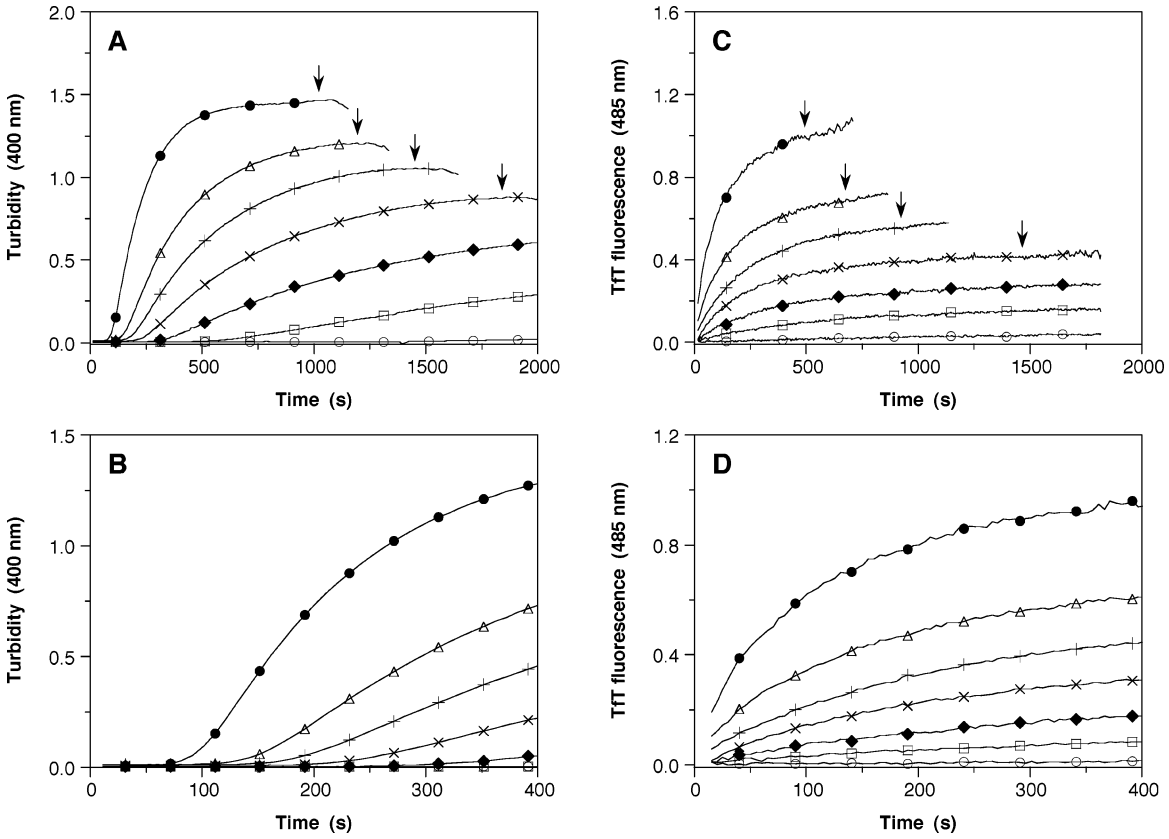

FIGURE 1: Dependence of M-TTR aggregation kinetics on M-TTR concentration. M-TTR aggregation was measured by the increase in turbidity (panels **A** and **B**) or in TfT fluorescence (panels **C** and **D**). Assays contained varying concentrations of M-TTR (0.05−0.4 mg/mL) at pH 4.4 and were carried out at 37 °C with no stirring (see Experimental Procedures for details). M-TTR concentrations in this representative experiment were 0.05 (○), 0.1 (□), 0.15 (◆), 0.2 (×), 0.25 (+), 0.3 (△), and 0.4 mg/mL (●). Solid lines represent the actual data points (collected at 10-s intervals for **A** and **B**, and 5-s intervals for **C** and **D**); symbols are used only to identify each line. The lower panels (**B** and **D**) show the same data as the upper panels (**A** and **C**, respectively), with an expanded time scale to emphasize differences in the initial rate measured by turbidity and TfT fluorescence. Arrows indicate where aggregates have become sufficiently large to interfere with the assays (see text for details).

FESP). All AFM supplies were obtained from Ted Pella, Inc. (Redding, CA).

(*B*) *Transmission Electron Microscopy.* Aliquots (5 μL) were placed on carbon-coated copper grids, and the solutions were allowed to stand for 2 min prior to removing the excess solution. Each grid was washed twice with deionized water and stained for 1 min with 2% uranyl acetate (in water); excess uranyl acetate was removed with filter paper. Controls ($t = 0$ s and buffer alone) for each experiment were prepared with the exact procedure detailed above and consisted of 0.2 mg/mL M-TTR in 10 mM sodium phosphate, 100 mM KCl, and 1 mM EDTA (pH 7.0), or of buffer alone (5 mM sodium phosphate and 100 mM sodium acetate, with 100 mM KCl and 1 mM EDTA, pH 4.4). EM samples were examined with a Phillips CM-100 transmission electron microscope, with an accelerating voltage of 100 kV. EM grids and other supplies were obtained from Electron Microscopy Sciences (Fort Washington, PA).

RESULTS

M-TTR Aggregation Kinetics. The kinetics of M-TTR aggregation mediated by acidic partial denaturation were examined by several biophysical methods. The rate and extent of aggregation are pH-dependent, with maximum aggregation occurring at pH 4.4 (*47*); hence, all of the experiments reported herein were carried out at pH 4.4. Figure 1 shows a representative experiment, where M-TTR aggregation was measured both by turbidity (panels A and B; same data plotted on two different scales) and by TfT binding (panels C and D; same data on different scales). The curves obtained by turbidity are sigmoidal in shape (Figure 1, panels A and B) and resemble those that are frequently reported for protein aggregation—at early times, there is an apparent lag, followed by a phase of rapid increase in turbidity and then a plateau. The reaction is dependent on the concentration of M-TTR in three ways: At higher M-TTR concentration, (1) the maximum amplitude, or endpoint, of the turbidity is increased, (2) the length of the apparent lag phase is shortened, and (3) the rate of reaction during the growth phase is accelerated. In contrast to the results obtained by turbidity, TfT fluorescence increases immediately upon mixing of M-TTR with low pH buffer (Figure 1, panels C and D). These reactions lack a lag phase, and the kinetic traces can be reasonably approximated by single or double exponential fits. TfT assays are also dependent on the concentration of M-TTR; increasing the M-TTR concentration results in a faster rate and a greater extent of aggregation. The time scale of M-TTR aggregation, as measured by these two techniques, is clearly different (Figure 1; compare panels B and D). For each M-TTR concentration examined, the reaction reaches greater than

half the maximal TfT amplitude before any increase in turbidity is detected.

Regardless of the method of detection, all aggregation reactions were carried out with no stirring. Although stirring can influence the rate of aggregation for some amyloidogenic proteins, preliminary experiments with M-TTR suggest that it has only a minimal effect on the observed rate of reaction in this case (data not shown). Nevertheless, we chose to study M-TTR aggregation under stagnant conditions because these are easier to replicate, facilitating the comparison of data obtained by different methods. Stagnant M-TTR aggregation reactions remain homogeneous suspensions essentially until reaching completion, when the aggregates become sufficiently large to settle out of solution. This phenomenon accounts for the observed decrease in turbidity (indicated by arrows in Figure 1A) and the apparent increase in TfT fluorescence (arrows in Figure 1C; this initial increase is followed by a decrease in fluorescence as the aggregates move through the light path). Although the data shown are truncated for clarity, reactions were allowed to proceed to completion (3600 s for turbidity assays or 1800 s for TfT assays) and were then mixed prior to determination of the reaction endpoint.

Turbidity Versus Thioflavin T Fluorescence Measurements. As described above, the kinetics of aggregation measured by turbidity and TfT fluorescence are clearly different. Detailed kinetic analysis of these data is complicated, since aggregation comprises many reactions occurring simultaneously. Furthermore, the form of the rate equation describing these reactions depends on what assumptions are made concerning the mechanism of aggregation. The shape of the curves obtained by the two methods is significantly different; however, neither the turbidity nor the TfT data is well fit by the model for nucleation-dependent polymerization (where either a cos t or a t^2 function approximates the first 10−20% of the reaction; ref *56*). Turbidity and TfT fluorescence assays were instead analyzed as follows: For each kinetic trace, the endpoint amplitude was measured, and the time required to reach 50% of the maximal amplitude (defined as t_{50}) was calculated. This simple yet robust method of analysis allows direct quantitative comparison of the aggregation kinetics at different protein concentrations and with different assays and provides insight into the reaction mechanism. The kinetic parameters obtained describe both the rate (t_{50}) and the extent (endpoint, or maximal amplitude) of reaction under a variety of conditions. Whereas the t_{50} for TfT reactions resembles a $t_{1/2}$ because the data are nearly exponential throughout the entire reaction, the turbidity t_{50} is influenced both by the length of the apparent lag and the rate during the growth phase of the reaction. Table 1 summarizes the t_{50} values obtained at varying M-TTR concentrations for turbidity and TfT assays in a representative experiment (from data in Figure 1). For each M-TTR concentration, the t_{50} obtained by turbidity is much longer than that calculated from TfT assays (∼3- to 8-fold in this experiment). Furthermore, the difference between the two t_{50}'s becomes more pronounced at lower M-TTR concentration. Another way of comparing these data is to determine the extent of reaction measured by each of these methods (i.e., turbidity or TfT) at the time point corresponding to the t_{50} determined by the other method (TfT or turbidity, respectively) under the same reaction conditions. These parameters are also summarized in Table 1. For each M-TTR concentration, the amount of turbidity observed is negligible (<1%) when the TfT reaction has proceeded to 50% completion. Conversely, TfT reactions are nearly complete (75−100%) by the time 50% of the maximum turbidity reaction is reached.

Table 1: Comparison of M-TTR Aggregation Kinetics[a]

	turbidity		TfT fluorescence	
[M-TTR] (mg/mL)	t_{50} (s)[b]	% completion at TfT t_{50}[c]	t_{50} (s)[b]	% completion at turbidity t_{50}[d]
0.05	3790	0.4	483	100
0.1	1527	<0.1	319	93.2
0.15	912	0.4	258	85.1
0.2	602	0.2	165	80.9
0.25	445	0.4	139	83.0
0.3	337	0.8	118	82.7
0.4	198	0.8	73	77.5

[a] The kinetics of aggregation of M-TTR at various concentrations are shown for a representative experiment, allowing the direct comparison of turbidity and TfT fluorescence assays. Reactions were carried out at pH 4.4 and 37 °C, as described in Experimental Procedures. [b] t_{50} represents the time required for the reaction to reach 50% completion. [c] Represents the extent of completion of the turbidity reaction at the time required to reach 50% of the maximum TfT fluorescence. [d] Represents the extent of completion of the TfT reaction at the time required to reach 50% of the maximum amplitude by turbidity.

Control reactions were carried out, to ensure that the presence of TfT in the assays does not affect the rate of aggregation. These reactions were carried out in microcentrifuge tubes in the absence of TfT. At various timepoints, aliquots were removed for analysis both by turbidity and by TfT. The results in these control experiments are qualitatively similar to those described above, namely that the increase in TfT precedes detectable turbidity (data not shown). Furthermore, the TfT fluorescence observed at discrete time points for reactions carried out in the absence of TfT is in good agreement with that obtained in continuous TfT assays. Small differences can be seen in the amplitude of the TfT signal, attributable to some fluorescence bleaching in the continuous experiments. The rate of reaction, however, is indistinguishable, indicating that the presence of TfT does not accelerate aggregation of M-TTR.

Nucleus Size and Critical Concentration. The same kinetic analysis described above (determination of reaction endpoints and t_{50}'s) can be used to determine the nucleus size and estimate the critical concentration for aggregation.

(*A*) *Nucleus Size*. Figure 2 shows the dependence of reaction t_{50} values (plotted as ln t_{50}) on the concentration of M-TTR (plotted as ln [M-TTR]). Both the turbidity (Figure 2A) and TfT data (Figure 2B) give straight lines, the slopes of which are related to the nucleus size, n^*. If aggregation is assumed to involve a preequilibrium corresponding to the formation of an oligomeric nucleus, followed by irreversible polymerization, then the slope obtained in this logarithmic plot (log−log) is equal to $-n^*/2$ (*59*). For the situation where aggregation is irreversible with no preequilibrium, implying that $n^* = 1$, the slope is equal to −1 (*59*). Linear regression of the data in Figure 2 yields a slope of −1.5 for turbidity and −1 for TfT assays. The somewhat steeper slope obtained by turbidity corresponds to a trimeric nucleus. A slope of −1, as obtained for the TfT data, is consistent with a dimeric

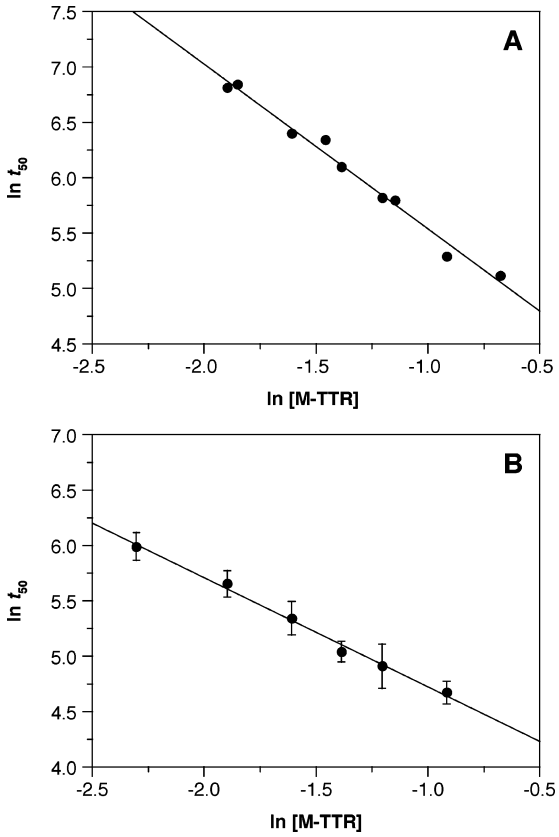

FIGURE 2: Determination of the nucleus size. The t_{50} (time to reach 50% maximal amplitude change) was calculated for each M-TTR concentration, using either turbidity data (panel **A**) or TfT fluorescence data (panel **B**). When plotted as a function of M-TTR concentration in a log−log plot, these data can be used to determine the nucleus size for aggregation (see text for details). (**A**) Data are shown for varying concentrations of M-TTR (0.15−0.5 mg/mL), derived from 2 separate experiments. A slope of -1.49 ± 0.07 was obtained by linear regression of the data. (**B**) Data points shown are averages of several experiments ($n = 3-7$, depending on the concentration), with the error bars indicating the standard deviation for each M-TTR concentration (0.1−0.4 mg/mL). The data were fit by linear regression, giving a slope of -0.98 ± 0.04.

nucleus for a nucleation-dependent polymerization; however, a slope of −1 is also the expectation for nonnucleated processes ($n^* = 1$; consistent with each step being both bimolecular and irreversible). Our data do not distinguish between these two possibilities (i.e., whether $n^* = 1$ or 2). In either case, the kinetics of aggregation do not show a high-order dependence on the M-TTR concentration; if this is a nucleated polymerization, the nucleus size is small.

(*B*) *Critical Concentration*. The dependence of the turbidity and TfT endpoints on the M-TTR concentration can be used to estimate the critical concentration for aggregation. Similar in concept to a critical micellar concentration, this parameter refers to the concentration of monomer below which no aggregation occurs (*57*−*60*). Figure 3 shows the plots of endpoints measured by turbidity (Figure 3A) and TfT (Figure 3B) as a function of M-TTR concentration. Two lines are shown in each plot, corresponding to reactions times of 1 and 24 h. For the lowest M-TTR concentrations examined (0.01 and 0.02 mg/mL), a reaction time of 24 h was necessary to detect any reaction; additionally, all of the concentrations show some increase in endpoint in this time range (1−24 h), especially in the turbidity assay. No further increase was observed at longer time points (24−48 h) for any of the reactions (data not shown). Linear regression of these data allows extrapolation to the *x*-intercept, which estimates the critical concentration (*58*). When the 24 h data are analyzed in this manner, the critical concentration for aggregation is calculated to be 0.012 and 0.005 mg/mL from turbidity and TfT assays, respectively.

By definition, the critical concentration is also equal to the equilibrium concentration of monomeric protein under amyloidogenic conditions, if the total protein concentration exceeds the critical concentration (*57*, *58*). The amount of M-TTR monomer remaining in solution during aggregation at long reaction times, as determined by analytical gel filtration, is shown in Figure 3. For all starting M-TTR concentrations, significant reaction is observed between 3 and 24 h, with the amount of monomer in solution decreasing as a function of time (Figure 3C). At 24 h, the reactions are approaching equilibrium, and the monomer concentration is ∼1−2 μg/mL. Figure 3D shows the concentration of monomer at 1 wk of reaction time for reactions containing varying concentrations of total M-TTR (0.01−0.4 mg/mL). This monomer concentration, 0.8 μg/mL, represents an upper limit on the critical concentration. In each of the reactions, the total M-TTR concentration is much greater than the critical concentration (∼12.5- to 500-fold), indicating that aggregation is thermodynamically favorable at all M-TTR concentrations examined. In the case of M-TTR aggregation, it is not clear whether the monomer concentration determined at long reaction times is truly a critical concentration, since this term is only meaningful for nucleated reactions. The lowest M-TTR concentration used here (0.01 mg/mL) is still more than an order of magnitude greater than the determined "critical concentration"; these comparatively high M-TTR concentrations may mask a nucleation step that would be apparent at total protein concentrations near the critical concentration. However, the sensitivity of all the assays employed is too low to allow studying aggregation at concentrations lower than ∼0.01 mg/mL.

Seeding Experiments. M-TTR aggregation reactions were incubated for varying lengths of time and added to reactions of fresh M-TTR, to test whether seeding increases the rate of M-TTR aggregation. Figure 4 shows a representative seeding experiment for M-TTR (0.2 mg/mL) where the seeds were derived from reactions only allowed to proceed for a short time. When seeding is examined by turbidity, small changes in the shape of the curves are obtained (Figure 4, panels A and B). Specifically, the turbidity observed immediately after initiation of the reaction is higher in the seeded reactions, consistent with the presence of preformed aggregates in the seed mixture. The turbidity at time zero in seeded reactions is dependent both on the amount of seed added (increasing with increasing weight percent seed) and the incubation time used for seed preparation (increasing with increasing incubation time). A second effect of the addition of seed is to shorten the length of the apparent lag phase. This is evidenced by an earlier and more gradual transition to the growth phase and translates to a shorter t_{50} in the seeded reactions (see Table 2 for a summary of t_{50}'s for seeded and unseeded reactions). A final effect is on the overall amplitude of the turbidity, which is slightly higher in the seeded reactions (Table 2). Despite these effects, the rate of reaction during the growth phase appears to be similar in all of the reactions for a particular M-TTR concentration,

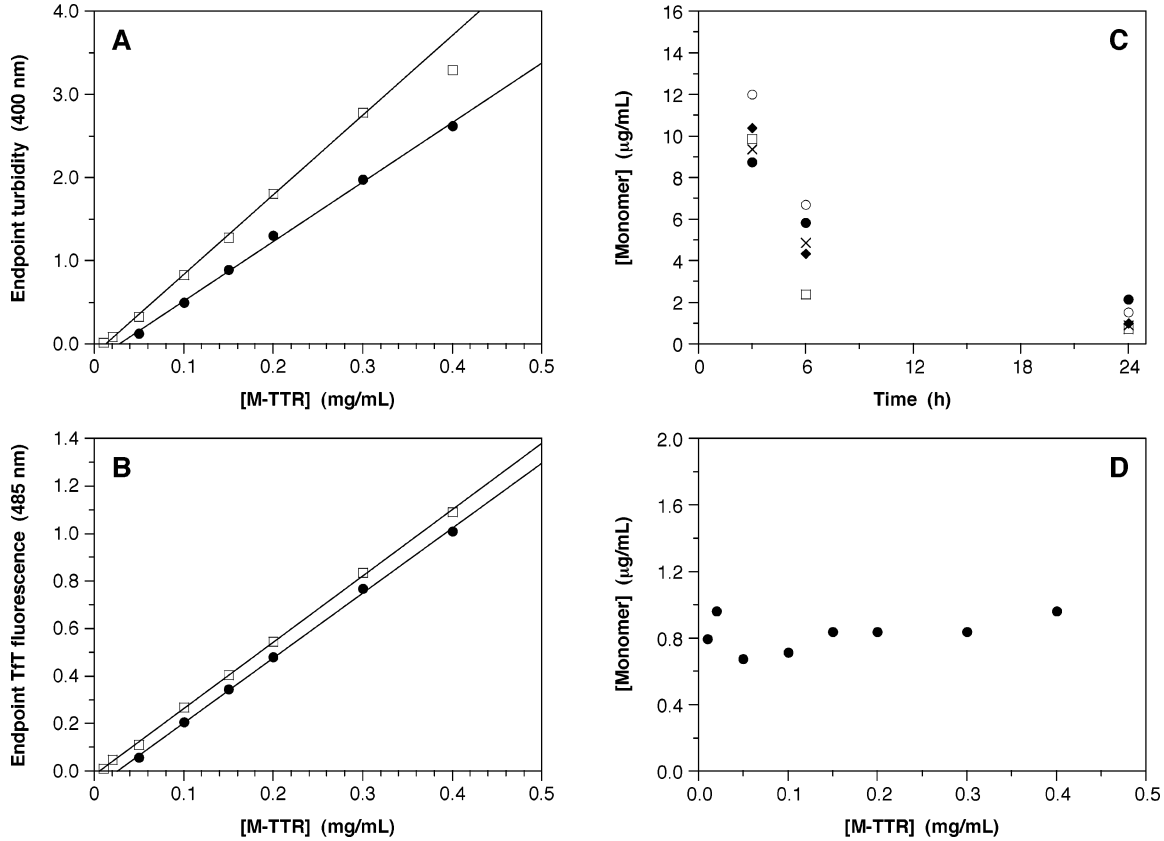

FIGURE 3: Determination of the critical concentration. (**A** and **B**) The critical concentration for M-TTR aggregation was estimated from aggregation reaction endpoints, with aggregation measured either by turbidity (panel **A**) or TfT fluorescence (panel **B**). A plot of the reaction endpoints as a function of M-TTR concentration (0.01−0.4 mg/mL) gives a straight line, where the critical concentration is estimated by the *x*-intercept (see text for details). (**A**) Data shown represent endpoint turbidity measured at reaction times of 1 h (●) or 24 h (□). The *x*-intercept for the 24 h data gives an estimated critical concentration for aggregation of 0.012 mg/mL M-TTR. (**B**) Endpoint TfT fluorescence data are shown for reaction times of 1 h (●) or 24 h (□). The critical concentration for aggregation determined from the 24 h data is 0.005 mg/mL M-TTR. (**C** and **D**) The critical concentration was also determined from the equilibrium concentration of M-TTR monomer in aggregating reactions, determined by analytical gel filtration at long reaction times. (**C**) The concentration of M-TTR monomer is shown as a function of time for reactions containing 0.05 (○), 0.1 (□), 0.15 (◆), 0.2 (×), and 0.4 mg/mL M-TTR (●), demonstrating that these reactions are approaching equilibrium at 24 h. (**D**) The monomer concentration determined at 1 wk of reaction time is shown for reactions containing 0.01−0.4 mg/mL M-TTR. The critical concentration determined by this method is ∼0.8 μg/mL for all reactions, regardless of the starting M-TTR concentration.

regardless of whether seed was present or not (i.e., the curves in Figure 4, panels A and B are parallel). Although the corresponding turbidity assays are not shown here, Table 2 summarizes the kinetic parameters determined for seeded and unseeded reactions for a range of M-TTR concentrations (0.05−0.4 mg/mL). At low concentration (0.05 and 0.1 mg/mL), the effect of seeding is minimal, whereas the changes in t_{50} and in the turbidity endpoint become more significant at higher M-TTR concentration (0.15−0.4 mg/mL).

In contrast to the effect of seeding on turbidity assays, traces of TfT fluorescence for the unseeded and seeded reactions are nearly superimposable (Figure 4, panels C and D). The only difference observed is in the amount of fluorescence at time zero. As noted for the turbidity results, this is attributed to the presence of TfT-positive aggregates in the seed mixtures; the magnitude of the TfT fluorescence at the start of the reaction is consistent with that expected for the given seed concentration and preparation time (as determined from the TfT fluorescence of the unseeded reaction at the time corresponding to the seed preparation time). The TfT endpoint is essentially unchanged by seeding, and the calculated t_{50} is either similar or slightly longer in the seeded reactions for the range of M-TTR concentrations examined (see Table 2). A longer t_{50} in seeded reactions is probably due to an effectively lower monomer M-TTR concentration, since some of the protein is already aggregated at initiation of these reactions.

The data shown in Figure 4 and Table 2 were obtained with seed preparation reactions that had been incubated for short times only (3 or 10 min). Although the data are not shown here, numerous additional seeding experiments were carried out to examine variables in the seed preparation. In most cases, the seed mixtures were only vortexed prior to addition to aggregation reactions. However, in several experiments, the seed mixtures were also sonicated to see if this resulted in any rate enhancement, because sonication can break up any preformed aggregates and thereby increase the number of sites (or ends) available to seed further polymerization. Seed mixtures were added to reactions in concentrations corresponding to 2, 5, or 10% (w/w) of the total M-TTR; the latter concentration is higher than those where seeding has been reported in other systems (typically 1−5%; refs *52*, *61*, *62*). Finally, the incubation period for seed preparation was also varied, from 1 min to 3 days, to test whether certain intermediates or aggregate structures formed along the reaction pathway are required to observe seeding. Regardless of the conditions used, the results obtained are qualitatively similar to those shown here: small

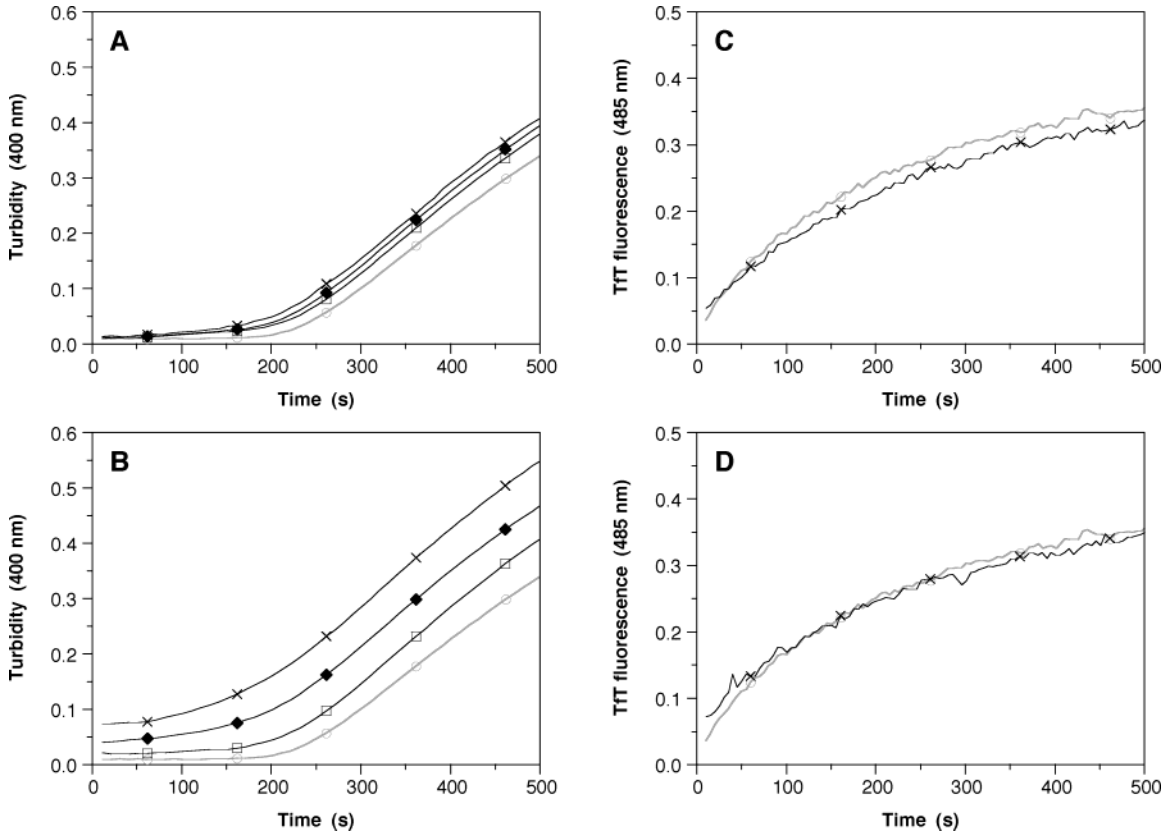

FIGURE 4: Effect of seeding on M-TTR aggregation kinetics. Aggregation reactions of 0.2 mg/mL M-TTR in the presence and absence of M-TTR seed were evaluated by turbidity (panels **A** and **B**) and by TfT fluorescence (panels **C** and **D**). Lines represent the actual data points, with symbols used to identify each line. Reactions contained 0 (○; shaded line), 2 (□), 5 (◆), or 10% seed (×); the concentration of total M-TTR (seed and fresh M-TTR) in each assay was 0.2 mg/mL (as detailed in Experimental Procedures). Seed reactions in this particular experiment were incubated for 3 min (panels **A** and **C**) or 10 min (panels **B** and **D**).

Table 2: Effect of Seeding on M-TTR Aggregation[a]

	unseeded reaction		seeded reaction	
[M-TTR] (mg/mL)	endpoint	t_{50} (s)	endpoint	t_{50} (s)
turbidity				
0.05	0.161	3790	0.161	3840
0.1	0.424	1527	0.470	1590
0.15	0.661	912	0.801	878
0.2	0.865	602	1.097	533
0.25	1.043	445	1.267	383
0.3	1.187	337	1.424	285
0.4	1.441	198	1.611	158
TfT fluorescence				
0.05	0.046	483	0.047	478
0.1	0.163	319	0.165	326
0.15	0.283	258	0.282	283
0.2	0.437	165	0.427	177
0.25	0.563	139	0.570	153
0.3	0.711	118	0.703	120
0.4	1.039	73	1.010	70

[a] Kinetic parameters determined for unseeded and seeded aggregation reactions at various M-TTR concentrations are summarized. All reactions were carried out at pH 4.4 and 37 °C. Seeded reactions contained 10% (w/w) M-TTR seed mixtures that had been incubated for 10 min (see Experimental Procedures for details).

differences result from seeding when the reactions are measured by turbidity, but no significant changes in the TfT kinetics were observed at any seed concentration or seed reaction time.

Analytical Gel Filtration. Because the kinetics of aggregation observed by turbidity and by TfT fluorescence are so dissimilar, we chose to also use analytical gel filtration to study the aggregation reaction. This method can directly measure the monomer concentration during aggregation and thus allows verification that the increase in TfT fluorescence is due to the formation of small aggregates at early reaction time points and not to the binding of TfT to an alternately folded monomeric state of M-TTR. A representative experiment is shown in Figure 5. Figure 5A shows several chromatograms obtained during aggregation of 0.2 mg/mL M-TTR. Analysis of M-TTR as purified (labeled 0 s) shows that this protein is >95% monomeric (elution volume 13.6 mL), with the balance of the protein eluting at a volume corresponding to a dimeric form (elution volume 10.5 mL). A small amount (<5%) of dimer can also be seen by SDS−PAGE analysis following cross-linking of M-TTR with glutaraldehyde (data not shown). No higher aggregates (e.g., tetramer) were observed in M-TTR preparations at the concentrations used in these experiments, consistent with previous results (*47*). Upon initiation of the aggregation reaction (by lowering the pH to 4.4), the monomer peak begins to decrease in intensity and a new peak appears (labeled "soluble" aggregate in Figure 5A because this material remains in solution if samples are centrifuged for 5 min at 16 000*g*). As the reaction progresses, the intensity of the soluble aggregate peak increases and its elution volume decreases (from ~8.8 mL at 30 s to ~7.9 mL at 180 s), indicating that both the concentration and the size of the aggregates are increasing. In reactions of 0.2 mg/mL M-TTR, the concentration of this peak reaches a maximum at a reaction time of ~200 s and subsequently begins to decrease.

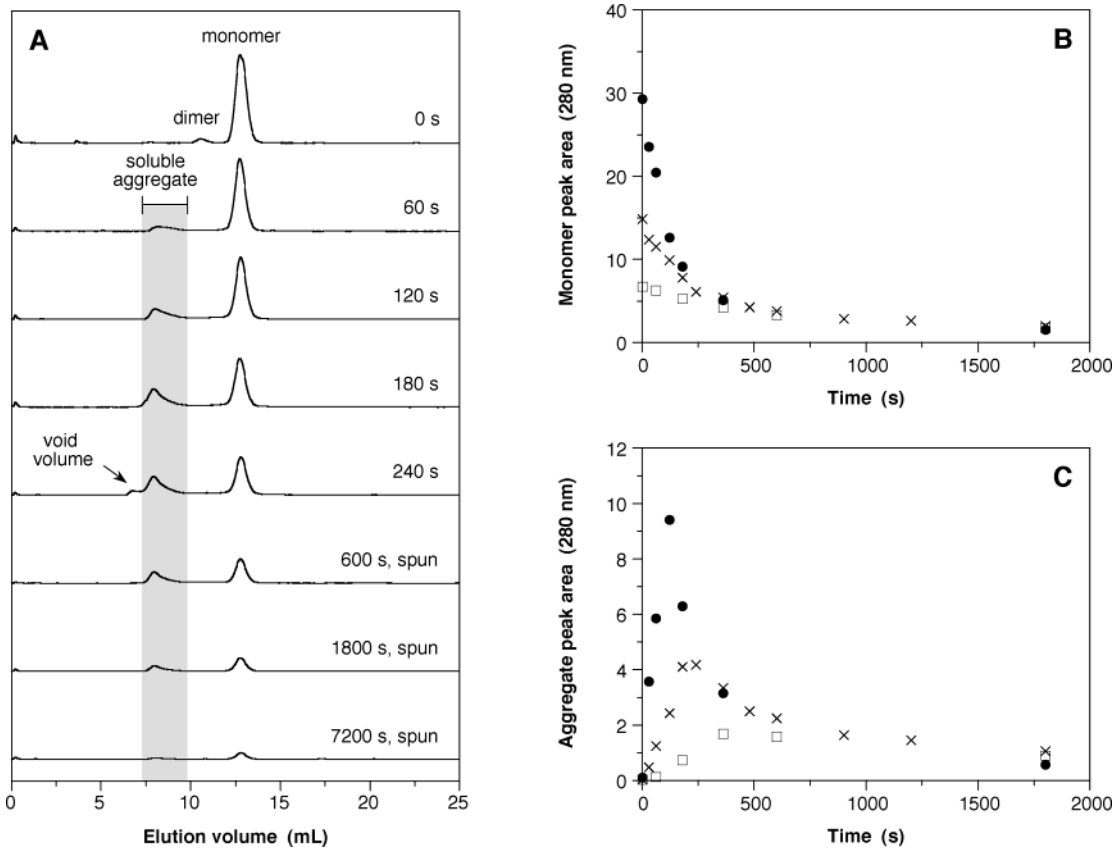

FIGURE 5: M-TTR aggregation measured by analytical gel filtration. Reactions contained M-TTR (0.1−0.4 mg/mL) at pH 4.4 and were incubated at 37 °C with no stirring prior to analysis by gel filtration. (**A**) Chromatograms of 0.2 mg/mL M-TTR at various times (0−7200 s, where 0 s is a pH 7.0 control) during the aggregation reaction are shown for a representative experiment. (**B** and **C**) The M-TTR monomer and soluble aggregate peaks in each chromatogram were integrated, and the peak areas are plotted as a function of reaction time. The disappearance of monomer (panel **B**) and the transient formation of soluble aggregates (panel **C**) are shown for reactions of 0.1 (□), 0.2 (×), and 0.4 mg/mL M-TTR (●).

At longer time points (t >180 s), some of the aggregates reach a size where they are no longer "soluble" (as defined above) and where they elute in the void volume (~7.0 mL) of the column (see 240 s trace). In this phase of the reaction, both the monomer peak and the soluble aggregate peak continue to decrease until essentially all of the M-TTR is present as large aggregates. At these long time points, the reaction mixtures are centrifuged prior to gel filtration to prevent clogging of the column; this centrifugation step accounts for the absence of large aggregates in the chromatograms. The monomer and soluble aggregate peaks in each chromatogram were integrated, and the peak areas were plotted as a function of reaction time.

The kinetics of monomer disappearance are shown in Figure 5B, and the formation and decay of soluble aggregates are shown in Figure 5C. Reactions were carried out at several M-TTR concentrations (chromatograms shown only for 0.2 mg/mL), and the chromatograms obtained were qualitatively similar to those shown for 0.2 mg/mL M-TTR in Figure 5A. As expected, these reactions also show a dependence on the M-TTR concentration, as described above for the turbidity and TfT assays. The disappearance of monomer is exponential in shape, and the rate of disappearance increases with increasing M-TTR concentration. The formation of soluble aggregates shows a similar dependence on M-TTR concentration; additionally, the maximal concentration of soluble aggregates obtained and the rate of disappearance of the soluble aggregates also increase with M-TTR concentration.

Aggregate Size and Morphology. The morphology of aggregates formed during the aggregation reaction was evaluated by microscopy; both AFM and EM were employed, to ensure that the results obtained were not a function of the particular adsorption properties of the surfaces used in each of these techniques. Figure 6 shows the progress of aggregation monitored by AFM for reactions containing 0.2 mg/mL M-TTR. The height mode images (Figure 6, panels A−D) represent topographic maps of the samples, where increasing brightness indicates greater feature height; amplitude mode images (Figure 6, panels E−H) are derivatives of the height mode images, where increasing brightness indicates greater damping of cantilever oscillation. Both image modes are shown, rather than the height mode alone, because some features are clearer in amplitude mode. The t = 0 s sample is a control containing 0.2 mg/mL M-TTR at pH 7.0 (Figure 6, panels A and E); the pitted appearance of the image is probably not due to TTR, but likely reflects imperfections in the mica surface. In either case, the overall variation in height in this sample is 0.5−1.0 nm, much smaller than that observed for the aggregated samples. The remaining samples contained 0.2 mg/mL M-TTR and were incubated at pH 4.4 and 37 °C for the lengths of time indicated (60−1800 s). In all of these samples, a high density of adsorbed protein is observed. Even at the earliest time points (≤180 s; Figure 6, panels B, C, F, and G), where no turbidity can be detected, the mica surface is completely covered with aggregated TTR. The aggregates appear to be

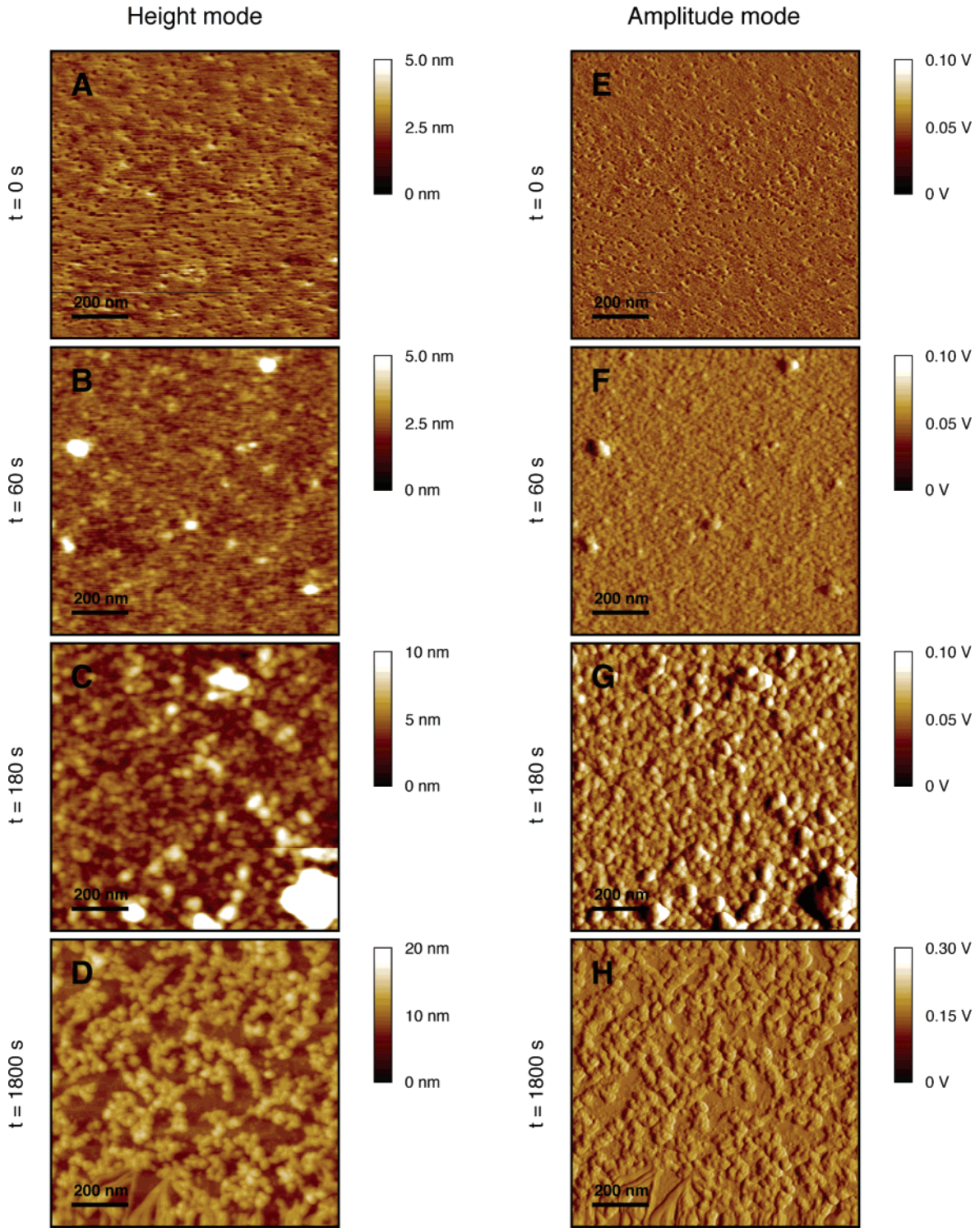

FIGURE 6: M-TTR aggregation monitored by AFM. AFM samples were prepared from reactions containing 0.2 mg/mL M-TTR at pH 4.4 and incubated at 37 °C with no stirring, with the exception of the $t = 0$ min sample, which is a pH 7.0 control containing 0.2 mg/mL M-TTR. AFM images were obtained in both height (panels **A**−**D**, where increasing brightness indicates greater feature height) and amplitude (panels **E**−**H**, where increasing brightness indicates greater damping of cantilever oscillation) modes and are shown at various reaction times (0−30 min). Each image represents a 1.0- × 1.0-μm area, and the appropriate height or amplitude scale bar is shown adjacent to each panel.

growing in all dimensions as the reaction progresses; in the *x*- and *y*-dimension, an increase in the periodicity of structures is observed, from ∼10 nm at 60 s (Figure 6F) to ∼25 nm at 180 s (Figure 6G); in the *z*-dimension, the height mode images show average variations increasing from 1−1.5 nm at 60 s (Figure 6B) to 2−3 nm at 180 s (Figure 6C) and to 4−8 nm at 1800 s (Figure 6D). These heights underestimate the actual heights of the aggregates, however, since there is no bare mica surface between the aggregates except in the 1800 s sample (Figure 6, panels D and H). Furthermore, the density of the adsorbed species also obscures the morphology of the aggregates. Nevertheless, AFM provides further evidence that M-TTR aggregation occurs immediately upon initiation of the reaction and that the size of the

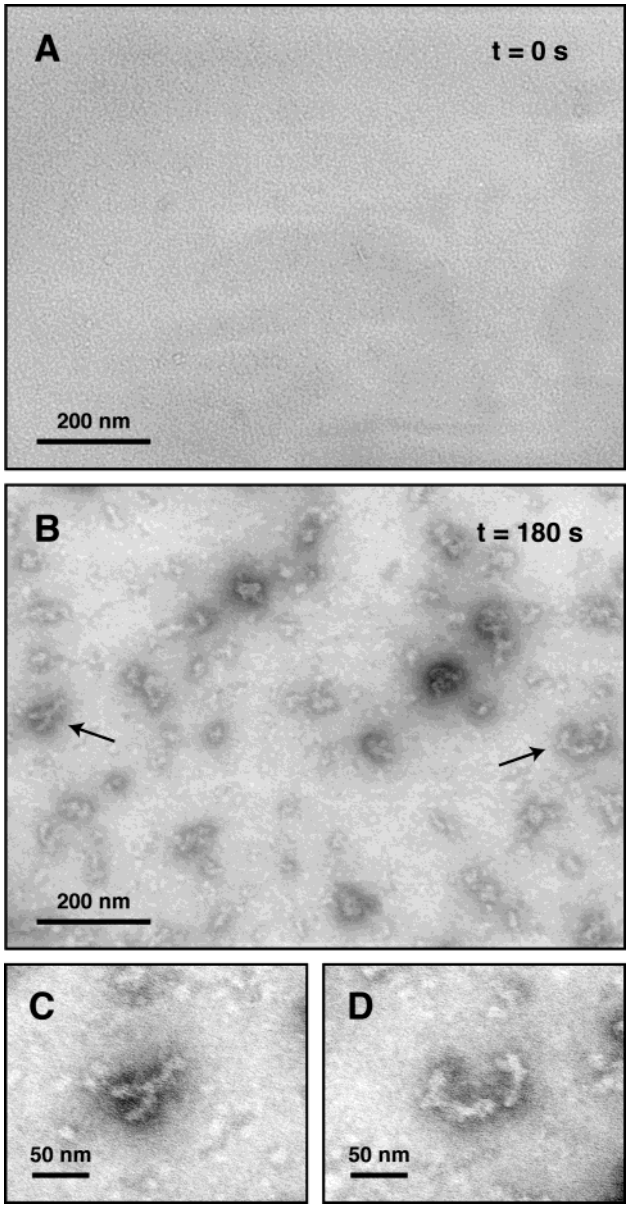

FIGURE 7: M-TTR aggregation monitored by EM. EM images of negatively stained M-TTR samples were obtained; samples contained 0.2 mg/mL M-TTR at pH 7.0 ($t = 0$ min control, panel **A**) or incubated at pH 4.4 and 37 °C for 3 min with no stirring (panels **B**−**D**). Images shown in panels **A** and **B** are photographs taken at 52 000× magnification. Small aggregates indicated by arrows in panel **B** are shown enlarged and with enhanced contrast in panels **C** and **D**.

aggregates increases as the reaction progresses. The EM images provide more structural information (Figure 7). The control sample (Figure 7A, $t = 0$ s) at pH 7.0 is devoid of any notable structures. In contrast, a number of elongated, flexible, and occasionally branched structures are apparent after 180 s of reaction time at pH 4.4 (Figure 7B), examples of which are indicated with arrows. These indicated areas are shown enlarged and with greater contrast in Figure 7, panels C and D. Although these aggregates are quite small, 7−10 nm in diameter and 25−75 nm in length, they resemble protofibrillar species previously observed with TTR and other amyloidogenic proteins (*50*, *63*−*68*). These structures disappear at longer time points, and no other species are observed. No mature fibrils of M-TTR were observed at any time point (up to 3600 s) by either microscopic technique.

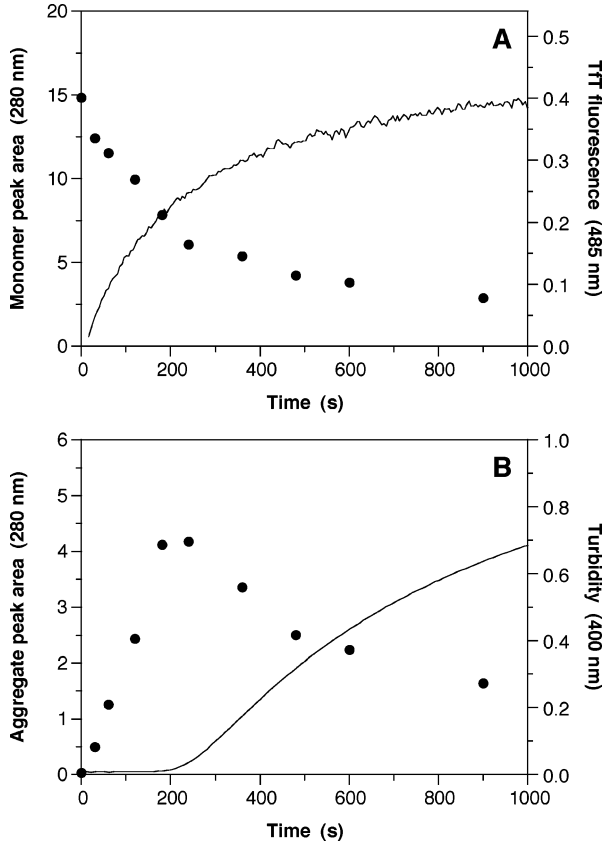

FIGURE 8: Comparison of M-TTR aggregation kinetics measured by various methods. The aggregation of 0.2 mg/mL M-TTR at pH 4.4 and 37 °C was measured by turbidity, TfT fluorescence, and analytical gel filtration. (**A**) The disappearance of M-TTR monomer measured by gel filtration (●, left *y*-axis) and the increase in TfT fluorescence (black line, right *y*-axis) are overlaid, showing that the rates of these two processes are comparable. (**B**) The formation of soluble aggregate measured by gel filtration (●, left *y*-axis) and the increase in turbidity (black line, right *y*-axis) are plotted together, to show that the increase in turbidity occurs on the same time scale as the disappearance of soluble aggregates.

Comparison of Aggregation Kinetics. Figure 8 shows representative turbidity, TfT, and analytical gel filtration data for the aggregation of 0.2 mg/mL M-TTR, plotted together to facilitate comparison of results obtained by the various methods. Overlaying the data in this manner demonstrates that the increase in TfT fluorescence occurs on the same time scale as the disappearance of monomer measured by gel filtration (Figure 8A), and that the increase in turbidity correlates with the disappearance of soluble aggregates (Figure 8B). The same correlations can be seen at all the M-TTR concentrations examined (0.1−0.4 mg/mL; data shown only for 0.2 mg/mL), demonstrating that the various assays provide complementary insight into the aggregation pathway (discussed below).

DISCUSSION

In this work, we have used a variety of methods to characterize TTR amyloidogenesis and to test whether this process is a nucleation-dependent polymerization. The model for this type of polymerization involves the intermediacy of a thermodynamic nucleus (*56*−*60*), which is by definition the highest energy species along the aggregation pathway and consequently the species that exists at the lowest concentration throughout the reaction. Scheme 1B shows an

adaptation of this model for the aggregation of tetrameric TTR, where tetramer dissociation is the overall rate-limiting step. Rate-limiting tetramer dissociation precludes the use of wtTTR to study the kinetics of TTR aggregation; hence, we have instead used an engineered monomeric variant, M-TTR (ref *47*; vide supra), to evaluate the mechanism of TTR amyloidogenesis. Although M-TTR was engineered by mutation of two residues, biophysical characterization (e.g., tertiary structure and structural stability) demonstrates that it behaves like the native wtTTR monomer and suggests that M-TTR is a reasonable model system for studying TTR amyloidogenesis. The existence of a thermodynamic nucleus in the aggregation pathway predicts that the system should exhibit the following characteristic kinetic behavior: (1) The time scale of the reaction should show a high-order dependence on the concentration of monomeric protein or peptide, (2) there should exist a concentration of monomer (the critical concentration), below which polymerization is so unfavorable that no reaction occurs, and (3) the rate of reaction should be dramatically increased upon the addition of preformed aggregates or "seeds", because seeding effectively bypasses the rate-limiting nucleation step.

Visual inspection of the kinetics of M-TTR aggregation at any given M-TTR concentration reveals differences between the timecourses observed and the predictions for a nucleated process. The absence of a lag phase in reactions monitored by TfT binding or gel filtration suggests that M-TTR aggregation is favorable immediately upon initiation. Although turbidity measurements give curves that have an apparent lag phase, these have a different curvature than that expected and cannot be satisfactorily fit by either of the approximations for nucleation-dependent polymerization described by Ferrone (*56*), in which a cos t or a t^2 function approximates the kinetics of the first 10−20% of the reaction. Further kinetic analysis indicates that the dependence of the rate of reaction on the concentration of M-TTR is not high-order. When aggregation is assessed by TfT, the dependence of the reaction timecourse is first-order on the M-TTR concentration, consistent either with a nucleus size of two or with a nonnucleated process where each step is both bimolecular and irreversible. The concentration dependence of turbidity assays is slightly higher order, consistent with a trimeric nucleus. The turbidity data are difficult to interpret, however, because turbidity measurements are not directly proportional to the total mass of polymerized protein (*58*). Determination of the critical concentration for M-TTR aggregation gives an upper limit of 0.8 μg/mL. This low concentration may not represent a true critical concentration, since this parameter is only meaningful for nucleated processes, but it does provide additional support that M-TTR amyloidogenesis is an energetically favorable process, at least at the M-TTR concentrations examined. A concentration of 0.8 μg/mL M-TTR corresponds to ~60 nM, which is several orders of magnitude lower than the critical concentration reported for Aβ aggregation (5−40 μM for Aβ_{1-40}; refs *53*, *69*−*71*). A recent report, however, suggests that the critical concentration for Aβ aggregation may be as low as 20 nM (*72*). The most compelling evidence that M-TTR aggregation is not nucleation-dependent comes from seeding experiments, which show that the addition of preformed seeds, prepared under a variety of conditions, does not accelerate aggregation. Although small differences in the shape of the turbidity curves are observed when seed mixtures are added to aggregation reactions, these likely reflect changes in the distribution of aggregate size rather than a true seeding phenomenon, which would represent an increase in the total mass of polymerized protein. This conclusion is reached on the basis of the concentration dependence of the observed "seeding". For a nucleation-dependent polymerization, the effect of seeding (at a given seed concentration) should be greatest at low protein concentration, where nucleus formation is very unfavorable, and where the observed rate of reaction in the absence of seed is very slow. Conversely, at high protein concentrations, nucleus formation is more favorable, and the increase in aggregation rate upon addition of preformed seed should be relatively smaller. In contrast to these expectations, our data show the opposite effect, namely that the differences in the reaction kinetics measured by turbidity become more pronounced with increasing M-TTR concentration (see Table 2 for a comparison of t_{50}'s for seeded and unseeded reactions). Additionally, TfT assays are completely insensitive to seeding under the same reaction conditions. These results suggest that the addition of seeds does not accelerate M-TTR aggregation but influences a secondary process that controls the distribution of aggregate size rather than the total amount of aggregated protein. An alternative explanation for the observed lack of seeding is that the "seeds" used in these experiments are structurally different from the nuclei required for aggregation and thus are not elongation-competent. This explanation seems unlikely, given the variety of conditions examined for seed maturation, but we cannot exclude the possibility that true seeds may form under different conditions.

Initially we used turbidity measurements and TfT binding assays to evaluate M-TTR amyloidogenesis, because both methods are frequently used to study fibril formation by amyloidogenic proteins and peptides. Although turbidity and TfT assays of M-TTR aggregation give significantly different results under identical experimental conditions, these apparently contradictory results in fact provide complementary insight into the aggregation pathway. TfT is an amyloid-selective dye whose fluorescence is proportional to the total amount of amyloid and is nearly insensitive to aggregate size (*73*); in contrast, turbidity does not distinguish between fibrillar and amorphous aggregates and is related to both the amount and size of the aggregates formed (*58*). A simple model that accounts for these limitations and is consistent with all our data, including analytical gel filtration and microscopy, is shown in Scheme 2. Partially denaturing conditions, such as the low pH used in these studies, enable M-TTR aggregation, which occurs essentially immediately upon initiation of the reaction. In the early phase of aggregation, the addition of M-TTR monomers to other monomers or oligomers predominates, leading to the formation of small aggregates (steps 1 and 2 in Scheme 2). These steps can be monitored by analytical gel filtration, both as the disappearance of monomer and as the formation of soluble aggregates, and by TfT assays. The correlation between the disappearance of M-TTR monomer and the increase in TfT fluorescence (Figure 8A) suggests that TfT assays are sensitive primarily to steps where aggregates grow by monomer addition, and that the minimal structure required for TfT binding (whether this represents amyloid or an amyloid-like structure has not been evaluated by other methods) is present even in the smallest aggregates. Both AFM (Figure 6) and EM (Figure 7) confirm that aggregates

Scheme 2: Model for M-TTR Amyloidogenesis[a]

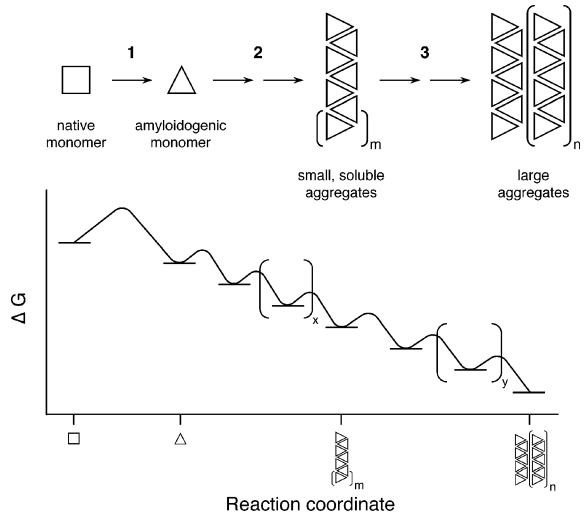

[a] Our results suggest this alternate model for M-TTR amyloidogenesis. When subjected to partially denaturing conditions, M-TTR misfolds into the amyloidogenic monomer (step **1**) and subsequently aggregates. Under these conditions, all of the steps along the pathway are energetically favorable, as illustrated by the free-energy diagram, and essentially irreversible. Nevertheless, M-TTR aggregation is characterized by at least two types of reactions. Initially, aggregation by the addition of monomers to other monomers or to oligomers predominates, leading to the accumulation of small aggregates (step **2**) that grow by monomeric increments, *m*. This phase of the reaction can be monitored by gel filtration (disappearance of monomer and increase in "soluble" aggregates) and by TfT fluorescence; the ability of these early aggregates to bind TfT suggests an amyloid or amyloid-like structure. As the reaction progresses, larger aggregates form primarily by secondary processes, such as the end-to-end or lateral assembly of existing aggregates (step **3**), rather than by monomer addition. Aggregate size increases dramatically in this phase, as evidenced by the rapid increase in turbidity. Only small increases in TfT binding are observed, however, because the total amount of polymerized M-TTR is not changed by these secondary processes. The number of individual steps in each phase of the aggregation reaction is not specified in our model, as indicated by the repeating units *x* and *y*.

are present at early time points (≤180 s for 0.2 mg/mL M-TTR) preceding the increase in turbidity. Although the morphology of the aggregates is not apparent from AFM, EM images show structures that resemble the protofibrillar species reported as early intermediates in the aggregation of other amyloidogenic proteins and peptides (*50*, *63*−*68*). Preliminary results using multi-angle light scattering indicate that the average molar mass at this same time point (180 s) is nearly 1 000 000 Da, consistent with a polymer of ∼70 monomer units (A. R. H. and J. W. K., unpublished observations). These data clearly show that the apparent lag in the turbidity traces is not due to a true lag in the aggregation kinetics, but rather to the low sensitivity of turbidity for small aggregates. The concentration of the intermediate aggregates reaches a maximum and subsequently decreases at a time that coincides with the rapid increase in turbidity (Figure 8B). Larger aggregates, which elute in the void volume of the gel filtration column and are no longer soluble after centrifugation, are formed in this phase of the aggregation process. The kinetics of monomer disappearance indicate that small and large aggregates continue to grow by the addition of monomers, much as they did in the initial phase of aggregation. However, existing aggregates also begin to grow by secondary processes, assembling by end-to-end or lateral association with other aggregates to form larger ones (step 3 in Scheme 2). As the reaction progresses and the monomer becomes increasingly depleted, these secondary processes begin to predominate. The large increases in turbidity observed in the latter stages of the reaction reflect a drastic growth in the aggregate size, as expected for this type of reaction. Only small increases in TfT binding are observed, however, because the total amount of polymerized M-TTR is unchanged by these secondary processes.

Although Scheme 2 superficially resembles Scheme 1B, our model does not invoke a thermodynamic nucleus, which is the central feature of the nucleation-dependent polymerization model. The small aggregates observed in our studies may represent a structure or substructure that is necessary for further growth into mature amyloid fibrils. However, these are not equivalent to a thermodynamic nucleus, which is defined as the highest energy species of the system and hence is present at the lowest concentration of all the possible species. This essential difference between the two models is illustrated in the corresponding free-energy diagrams in Schemes 1B and 2. A consequence of the assumptions for nucleation-dependent polymerization, where steps preceding nucleus formation are characterized by unfavorable equilibria and those following nucleation are favorable, is that the rate of nucleation shows a high-order dependence on the concentration of monomeric protein, whereas the rate of elongation after nucleus formation shows only a first-order dependence on the monomer concentration. In contrast, M-TTR amyloidogenesis appears to be a downhill polymerization, where each step is essentially irreversible (with a first-order monomer concentration dependence) and where the highest energy species under partially denaturing conditions is the native monomer. A large number of relatively small aggregates, as opposed to the long fibrils often observed in other aggregating systems, are formed during TTR aggregation in vitro, as evidenced by the microscopy results reported here for M-TTR and in previous experiments with wild-type and L55P TTR (*37*, *47*, *50*, *65*, *67*). This observation is consistent with Scheme 2, where the rates for the formation of new aggregates and the growth of existing ones are comparable. Although amyloidogenesis is often assumed to proceed by a nucleation-dependent polymerization mechanism, recent experimental results with other aggregating systems (e.g., Aβ, IAPP, polyglutamine peptides, immunoglobulin light chain, prion protein) indicate that the simple nucleation-dependent model (Scheme 1A) does not adequately describe all of the features and kinetic behavior of these reactions either. A number of alternative models—involving metastable oligomeric species, off-pathway intermediates, secondary nucleation, or branched pathways—have been proposed to explain these observations (*61*−*64*, *74*−*78*).

Our studies provide insight into the M-TTR aggregation pathway in vitro, but further experiments are needed to address the relationship between this in vitro mechanism and TTR amyloidogenesis in vivo. Partially denaturing conditions, such as the low pH used in these experiments, are required to observe aggregation of TTR on a reasonable laboratory time scale. However, the physiological context in which TTR amyloid formation occurs in patients is not known. A different mechanism of amyloidogenesis than that described herein for in vitro reactions may prevail in vivo, since the specific solution conditions can dramatically influence aggregation reactions (for example, see refs *75*,

76, *79*, *80*). Furthermore, the in vivo concentration of TTR monomer must also be considered. Although the normal concentration of TTR in human plasma (0.1−0.4 mg/mL) is in the same range as the concentrations used for our in vitro studies, most of the TTR in vivo should be present as the native tetramer. A low TTR monomer concentration probably prevents amyloid formation under normal physiological conditions; however, small changes in the tetramer−monomer equilibrium may be sufficient to trigger the onset of amyloidogenesis. For example, many FAP/FAC variants of TTR have a decreased quaternary structural stability that appears to be correlated with their amyloidogenicity (*33*−*40*). Additionally, since a significant percentage of the elderly develop SSA, it is possible that age-dependent increases in the concentration of monomeric TTR may be responsible for the development of this disease as well. Age-dependent perturbations to the tetramer−monomer equilibrium could arise from diverse factors, as previously discussed (*81*). Finally, it is conceivable that seeding could accelerate amyloidogenesis in vivo, if the TTR monomer concentration is similar to the critical concentration for aggregation. Under such conditions, which are difficult to study in the laboratory, TTR amyloidogenesis may become nucleation-dependent and hence seedable. This potential change in mechanism would offer an explanation for some aspects of the pathology of TTR amyloid disease (e.g., relatively rapid onset of symptoms and the genetic anticipation observed with some variants).

This work also has implications for the development of therapeutic strategies for TTR amyloid disease. Although several approaches have been discussed (*21*, *28*, *82*), the only currently available treatment for patients with variant TTR disease (FAP/FAC) is liver transplantation. This approach is a crude method of gene therapy; because most of the plasma TTR is synthesized in the liver, transplantation results in the replacement of variant TTR with wtTTR (from wtTTR donor liver), which in principle should halt and perhaps reverse the progression of disease in these patients. This therapy has been partially successful in some cases (*83*−*85*), but is not the most desirable approach because of the invasive nature of the treatment and the potential for complications associated with the procedure. Furthermore, transplantation can only be used in patients where a mutation is responsible for disease (FAP/FAC); no treatment is yet available for patients with wild-type TTR disease (SSA). Other strategies focus on intervention at various stages of amyloidogenesis. Recent studies have shown that early intermediates in the aggregation pathway are cytotoxic and may be responsible for the observed symptoms of the associated diseases (*10*, *12*, *20*). Inhibition of the initial stages of amyloidogenesis would thus be desirable, but the observed efficiency of M-TTR aggregation suggests that this will be a difficult goal to achieve. An alternative strategy aimed at decreasing the fibril load in vivo by depolymerization of existing fibrils (*82*) may not be effective at alleviating disease symptoms, since this strategy would result in an increase in smaller aggregates that might be more toxic than the fibrils themselves. A final approach for the treatment of TTR amyloid disease involves the stabilization of the native tetrameric state of TTR and has been a focus of our laboratory for several years (*86*−*88*). Prevention of tetramer dissociation provides the most attractive target for inhibiting TTR aggregation, because this step is rate-limiting for TTR amyloidogenesis (*46*, *47*). The TTR tetramer can be stabilized by the binding of its native ligands, thyroxine and retinol binding protein, both of which suppress fibril formation in vitro (*81*, *86*). Our laboratory has synthesized a number of small molecules that bind in the thyroxine-binding sites, thereby stabilizing the TTR tetramer and inhibiting amyloidogenesis (*86*−*88*). This approach has led to the discovery of several promising compounds, and initial clinical studies are underway to test whether this therapeutic approach may be useful in the treatment of patients with TTR amyloid disease.

In summary, the mechanism of M-TTR amyloidogenesis under partially denaturing conditions in vitro is best represented as a downhill polymerization that proceeds without the involvement of a high-energy multimeric nucleus. M-TTR aggregation is a complex, multistep process, but all the steps in the reaction appear to be thermodynamically favorable. TTR dissociation into its component monomers and partial unfolding of the monomers are required to generate the amyloidogenic intermediate. Once formed, this misfolded monomer efficiently self-assembles into fibrillar and other aggregates that may play a role in the pathology of TTR amyloid disease. Amyloid formation by M-TTR in vitro is strikingly different from that characterized for several amyloidogenic peptides, such as Aβ and IAPP, whose aggregation requires a thermodynamic nucleus. The observed differences may be attributable to whether the polypeptide involved is a folded protein (TTR) or an unstructured peptide (Aβ or IAPP), because the steps leading to the formation of an aggregation-competent intermediate in the two cases are fundamentally different. Although additional experiments are required to evaluate whether downhill polymerization is a general mechanism for amyloid formation by natively folded proteins or is unique to TTR, it is clear that amyloidogenesis does not proceed by a common mechanism for all amyloidogenic proteins and peptides.

ACKNOWLEDGMENT

We thank Dr. Songpon Deechongkit for obtaining the electron microscopy images and Maria Dendle for purifying some of the M-TTR used in these experiments. We also thank Prof. Reza Ghadiri at The Scripps Research Institute for the use of his atomic force microscope.

REFERENCES

1. Sipe, J. D. (1994) Amyloidosis, *Crit. Rev. Clin. Lab. Sci. 31*, 325−354.
2. Kelly, J. W. (1996) Alternative conformations of amyloidogenic proteins govern their behavior, *Curr. Opin. Struct. Biol. 6*, 11−17.
3. Westermark, P. (1997) Classification of amyloid fibril proteins and their precursors: an ongoing discussion, *Amyloid 4*, 216−218.
4. Merlini, G., and Bellotti, V. (2003) Molecular mechanisms of amyloidosis, *N. Engl. J. Med. 349*, 583−596.
5. Selkoe, D. J. (2001) Alzheimer's disease: genes, proteins, and therapy, *Physiol. Rev. 81*, 741−766.
6. Hardy, J. A., and Higgins, G. A. (1992) Alzheimer's disease: the amyloid cascade hypothesis, *Science 256*, 184−185.
7. Hardy, J., and Selkoe, D. J. (2002) The amyloid hypothesis of Alzheimer's disease: progress and problems on the road to therapeutics, *Science 297*, 353−356.
8. Sipe, J. D., and Cohen, A. S. (2000) Review: history of the amyloid fibril, *J. Struct. Biol. 130*, 88−98.
9. Dobson, C. M. (1999) Protein misfolding, evolution and disease, *Trends Biochem. Sci. 24*, 329−332.

10. McLean, C. A., Cherny, R. A., Fraser, F. W., Fuller, S. J., Smith, M. J., Beyreuther, K., Bush, A. I., and Masters, C. L. (1999) Soluble pool of Aβ amyloid as a determinant of severity of neurodegeneration in Alzheimer's disease, *Ann. Neurol. 46*, 860−866.
11. Lue, L. F., Kuo, Y. M., Roher, A. E., Brachova, L., Shen, Y., Sue, L., Beach, T., Kurth, J. H., Rydel, R. E., and Rogers, J. (1999) Soluble amyloid β peptide concentration as a predictor of synaptic change in Alzheimer's disease, *Am. J. Pathol. 155*, 853−862.
12. Sousa, M. M., Cardoso, I., Fernandes, R., Guimaraes, A., and Saraiva, M. J. (2001) Deposition of transthyretin in early stages of familial amyloidotic polyneuropathy: Evidence for toxicity of nonfibrillar aggregates, *Am. J. Pathol. 159*, 1993−2000.
13. Hartley, D. M., Walsh, D. M., Ye, C. P., Diehl, T., Vasquez, S., Vassilev, P. M., Teplow, D. B., and Selkoe, D. J. (1999) Protofibrillar intermediates of amyloid beta-protein induce acute electrophysiological changes and progressive neurotoxicity in cortical neurons, *J. Neurosci. 19*, 8876−8884.
14. Janson, J., Ashley, R. H., Harrison, D., McIntyre, S., and Butler, P. C. (1999) The mechanism of islet amyloid polypeptide toxicity is membrane disruption by intermediate-sized toxic amyloid particles, *Diabetes 48*, 491−498.
15. Walsh, D. M., Hartley, D. M., Condron, M. M., Selkoe, D. J., and Teplow, D. B. (2001) In vitro studies of amyloid beta-protein fibril assembly and toxicity provide clues to the aetiology of Flemish variant (Ala692→Gly) Alzheimer's disease, *Biochem. J. 355*, 869−877.
16. Walsh, D. M., Klyubin, I., Fadeeva, J. V., Cullen, W. K., Anwyl, R., Wolfe, M. S., Rowan, M. J., and Selkoe, D. J. (2002) Naturally secreted oligomers of amyloid beta protein potently inhibit hippocampal long-term potentiation in vivo, *Nature 416*, 535−539.
17. Dahlgren, K. N., Manelli, A. M., Stine, W. B., Jr., Baker, L. K., Krafft, G. A., and LaDu, M. J. (2002) Oligomeric and fibrillar species of amyloid-beta peptides differentially affect neuronal viability, *J. Biol. Chem. 277*, 32046−32053.
18. Bucciantini, M., Giannoni, E., Chiti, F., Baroni, F., Formigli, L., Zurdo, J., Taddei, N., Ramponi, G., Dobson, C. M., and Stefani, M. (2002) Inherent toxicity of aggregates implies a common mechanism for protein misfolding diseases, *Nature 416*, 507−511.
19. Hoshi, M., Sato, M., Matsumoto, S., Noguchi, A., Yasutake, K., Yoshida, N., and Sato, K. (2003) Spherical aggregates of beta-amyloid (amylospheroid) show high neurotoxicity and activate tau protein kinase I/glycogen synthase kinase-3beta, *Proc. Natl. Acad. Sci. U.S.A. 100*, 6370−6375.
20. Klein, W. L., Krafft, G. A., and Finch, C. E. (2001) Targeting small Abeta oligomers: the solution to an Alzheimer's disease conundrum?, *Trends Neurosci. 24*, 219−224.
21. Cohen, F. E., and Kelly, J. W. (2003) Therapeutic approaches to protein-misfolding diseases, *Nature 426*, 905−909.
22. Blake, C. C., Swan, I. D., Rerat, C., Berthou, J., Laurent, A., and Rerat, B. (1971) An X-ray study of the subunit structure of prealbumin, *J. Mol. Biol. 61*, 217−224.
23. Blake, C. C., Geisow, M. J., Oatley, S. J., Rerat, B., and Rerat, C. (1978) Structure of prealbumin: secondary, tertiary, and quaternary interactions determined by Fourier refinement at 1.8 A, *J. Mol. Biol. 121*, 339−356.
24. Hamilton, J. A., and Benson, M. D. (2001) Transthyretin: a review from a structural perspective, *Cell. Mol. Life Sci. 58*, 1491−1521.
25. Cornwell, G. G., III, Sletten, K., Johansson, B., and Westermark, P. (1988) Evidence that the amyloid fibril protein in senile systemic amyloidosis is derived from normal prealbumin, *Biochem. Biophys. Res. Commun. 154*, 648−653.
26. Westermark, P., Sletten, K., Johansson, B., and Cornwell, G. G., III (1990) Fibril in senile systemic amyloidosis is derived from normal transthyretin, *Proc. Natl. Acad. Sci. U.S.A. 87*, 2843−2845.
27. Benson, M. D. (1989) Familial amyloidotic polyneuropathy, *Trends Biochem. Sci. 12*, 88−92.
28. Damas, A. M., and Saraiva, M. J. (2000) Review: TTR amyloidosis-structural features leading to protein aggregation and their implications on therapeutic strategies, *J. Struct. Biol. 130*, 290−299.
29. Saraiva, M. J. (2001) Transthyretin mutations in hyperthyroxinemia and amyloid diseases, *Hum. Mutat. 17*, 493−503.
30. Terry, C. J., Damas, A. M., Oliveira, P., Saraiva, M. J. M., Alves, I. L., Costa, P. P., Matias, P. M., Sakaki, Y., and Blake, C. C. F. (1993) Structure of Met30 variant of transthyretin and its amyloidogenic implications, *EMBO J. 12*, 735−741.
31. Steinrauf, L. K., Cao, Y., Hamilton, J., Murrell, J., Liepnieks, J. J., and Benson, M. D. (1991) Preparation and crystallization of human transthyretin (prealbumin) variants, *Biochem. Biophys. Res. Commun. 179*, 804−809.
32. Hornberg, A., Eneqvist, T., Olofsson, A., Lundgren, E., and Sauer-Eriksson, A. E. (2000) A comparative analysis of 23 structures of the amyloidogenic protein transthyretin, *J. Mol. Biol. 302*, 649−669.
33. McCutchen, S. L., Colon, W., and Kelly, J. W. (1993) Transthyretin mutation Leu-55-Pro significantly alters tetramer stability and increases amyloidogenicity, *Biochemistry 32*, 12119−12127.
34. McCutchen, S. L., Lai, Z., Miroy, G. J., Kelly, J. W., and Colon, W. (1995) Comparison of lethal and nonlethal transthyretin variants and their relationship to amyloid disease, *Biochemistry 34*, 13527−13536.
35. Bonifacio, M. J., Sakaki, Y., and Saraiva, M. J. (1996) In vitro amyloid fibril formation from transthyretin: the influence of ions and the amyloidogenicity of TTR variants, *Biochim. Biophys. Acta 1316*, 35−42.
36. Quintas, A., Saraiva, M. J., and Brito, R. M. (1997) The amyloidogenic potential of transthyretin variants correlates with their tendency to aggregate in solution, *FEBS Lett. 418*, 297−300.
37. Lashuel, H. A., Lai, Z., and Kelly, J. W. (1998) Characterization of the transthyretin acid denaturation pathways by analytical ultracentrifugation: implications for wild-type, V30M, and L55P amyloid fibril formation, *Biochemistry 37*, 17851−17864.
38. Shnyrov, V. L., Villar, E., Zhadan, G. G., Sanchez-Ruiz, J. M., Quintas, A., Saraiva, M. J., and Brito, R. M. (2000) Comparative calorimetric study of non-amyloidogenic and amyloidogenic variants of the homotetrameric protein transthyretin, *Biophys. Chem. 88*, 61−67.
39. Jiang, X., Buxbaum, J. N., and Kelly, J. W. (2001) The V122I cardiomyopathy variant of transthyretin increases the velocity of rate-limiting tetramer dissociation, resulting in accelerated amyloidosis, *Proc. Natl. Acad. Sci. U.S.A. 98*, 14943−14948.
40. Hammarstrom, P., Jiang, X., Hurshman, A. R., Powers, E. T., and Kelly, J. W. (2002) Sequence-dependent denaturation energetics: A major determinant in amyloid disease diversity, *Proc. Natl. Acad. Sci. U.S.A. 99*, 16427−16432.
41. Longo Alves, I., Hays, M. T., and Saraiva, M. J. (1997) Comparative stability and clearance of [Met30]transthyretin and [Met119]transthyretin, *Eur. J. Biochem. 249*, 662−668.
42. Hammarstrom, P., Schneider, F., and Kelly, J. W. (2001) Trans-suppression of misfolding in an amyloid disease, *Science 293*, 2459−2462.
43. Hammarstrom, P., Wiseman, R. L., Powers, E. T., and Kelly, J. W. (2003) Prevention of transthyretin amyloid disease by changing protein misfolding energetics, *Science 299*, 713−716.
44. Coelho, T., Carvalho, M., Saraiva, M. J., Alves, I. L., Almeida, M. R., and Costa, P. P. (1993) A strikingly benign evolution of FAP in an individual compound heterozygote for two TTR mutations: TTR Met30 and TTR Met119, *J. Rheumatol. 20*, 179.
45. Coelho, T., Chorao, R., Sousa, A., Alves, I. L., Torres, M. F., and Saraiva, M. J. (1996) Compound heterozygotes of transthyretin Met30 and transthyretin Met119 are protected from the devastating effects of Familial Amyloid Polyneuropathy, *Neuromuscul. Disord. 6*, 27−32.
46. Lai, Z., Colon, W., and Kelly, J. W. (1996) The acid-mediated denaturation pathway of transthyretin yields a conformational intermediate that can self-assemble into amyloid, *Biochemistry 35*, 6470−6482.
47. Jiang, X., Smith, C. S., Petrassi, H. M., Hammarström, P., White, J. T., Sacchettini, J. C., and Kelly, J. W. (2001) An engineered transthyretin monomer that is nonamyloidogenic, unless it is partially denatured, *Biochemistry 40*, 11442−11452.
48. Colon, W., and Kelly, J. W. (1992) Partial denaturation of transthyretin is sufficient for amyloid fibril formation in vitro, *Biochemistry 31*, 8654−8660.
49. Quintas, A., Saraiva, M. J., and Brito, R. M. (1999) The tetrameric protein transthyretin dissociates to a non-native monomer in solution. A novel model for amyloidogenesis, *J. Biol. Chem. 274*, 32943−32949.
50. Quintas, A., Vaz, D. C., Cardoso, I., Saraiva, M. J., and Brito, R. M. (2001) Tetramer dissociation and monomer partial unfolding precedes protofibril formation in amyloidogenic transthyretin variants, *J. Biol. Chem. 276*, 27207−27213.

51. Liu, K., Cho, H. S., Lashuel, H. A., Kelly, J. W., and Wemmer, D. E. (2000) A glimpse of a possible amyloidogenic intermediate of transthyretin, *Nat. Struct. Biol. 7*, 754−757.
52. Jarrett, J. T., and Lansbury, P. T., Jr. (1992) Amyloid fibril formation requires a chemically discriminating nucleation event: studies of an amyloidogenic sequence from the bacterial protein OsmB, *Biochemistry 31*, 12345−12352.
53. Jarrett, J. T., Berger, E. P., and Lansbury, P. T., Jr. (1993) The carboxy terminus of the beta amyloid protein is critical for the seeding of amyloid formation: implications for the pathogenesis of Alzheimer's disease, *Biochemistry 32*, 4693−4697.
54. Lomakin, A., Chung, D. S., Benedek, G. B., Kirschner, D. A., and Teplow, D. B. (1996) On the nucleation and growth of amyloid beta-protein fibrils: detection of nuclei and quantitation of rate constants, *Proc. Natl. Acad. Sci. U.S.A. 93*, 1125−1129.
55. Lomakin, A., Teplow, D. B., Kirschner, D. A., and Benedek, G. B. (1997) Kinetic theory of fibrillogenesis of amyloid beta-protein, *Proc. Natl. Acad. Sci. U.S.A. 94*, 7942−7947.
56. Ferrone, F. (1999) Analysis of protein aggregation kinetics, *Methods Enzymol. 309*, 256−274.
57. Harper, J. D., and Lansbury, P. T., Jr. (1997) Models of amyloid seeding in Alzheimer's disease and scrapie: mechanistic truths and physiological consequences of the time-dependent solubility of amyloid proteins, *Annu. Rev. Biochem. 66*, 385−407.
58. Andreu, J. M., and Timasheff, S. N. (1986) The measurement of cooperative protein self-assembly by turbidity and other techniques, *Methods Enzymol. 130*, 47−59.
59. Goldstein, R. F., and Stryer, L. (1986) Cooperative polymerization reactions. Analytical approximations, numerical examples, and experimental strategy, *Biophys. J. 50*, 583−599.
60. Oosawa, F., and Asakura, S. (1975) *Thermodynamics of the Polymerization of Protein*, Academic Press, London.
61. Chen, S., Ferrone, F. A., and Wetzel, R. (2002) Huntington's disease age-of-onset linked to polyglutamine aggregation nucleation, *Proc. Natl. Acad. Sci. U.S.A. 99*, 11884−11889.
62. Padrick, S. B., and Miranker, A. D. (2002) Islet amyloid: phase partitioning and secondary nucleation are central to the mechanism of fibrillogenesis, *Biochemistry 41*, 4694−4703.
63. Harper, J. D., Wong, S. S., Lieber, C. M., and Lansbury, P. T. (1997) Observation of metastable Aβ amyloid protofibrils by atomic force microscopy, *Chem. Biol. 4*, 119−125.
64. Walsh, D. M., Lomakin, A., Benedek, G. B., Condron, M. M., and Teplow, D. B. (1997) Amyloid beta-protein fibrillogenesis. Detection of a protofibrillar intermediate, *J. Biol. Chem. 272*, 22364−22372.
65. Lashuel, H. A., Wurth, C., Woo, L., and Kelly, J. W. (1999) The most pathogenic transthyretin variant, L55P, forms amyloid fibrils under acidic conditions and protofilaments under physiological conditions, *Biochemistry 38*, 13560−13573.
66. Nielsen, E. H., Nybo, M., and Svehag, S.-E. (1999) Electron microscopy of prefibrillar structures and amyloid fibrils, *Methods Enzymol. 309*, 491−496.
67. Cardoso, I., Goldsbury, C. S., Muller, S. A., Olivieri, V., Wirtz, S., Damas, A. M., Aebi, U., and Saraiva, M. J. (2002) Transthyretin fibrillogenesis entails the assembly of monomers: a molecular model for in vitro assembled transthyretin amyloid-like fibrils, *J. Mol. Biol. 317*, 683−695.
68. Kheterpal, I., Lashuel, H. A., Hartley, D. M., Walz, T., Lansbury, P. T., Jr., and Wetzel, R. (2003) Abeta protofibrils possess a stable core structure resistant to hydrogen exchange, *Biochemistry 42*, 14092−14098.
69. Evans, K. C., Berger, E. P., Cho, C. G., Weisgraber, K. H., and Lansbury, P. T., Jr. (1995) Apolipoprotein E is a kinetic but not a thermodynamic inhibitor of amyloid formation: implications for the pathogenesis and treatment of Alzheimer disease, *Proc. Natl. Acad. Sci. U.S.A. 92*, 763−767.
70. Seelig, J., Lehrmann, R., and Terzi, E. (1995) Domain formation induced by lipid-ion and lipid-peptide interactions, *Mol. Membr. Biol. 12*, 51−57.
71. Sengupta, P., Garai, K., Sahoo, B., Shi, Y., Callaway, D. J., and Maiti, S. (2003) The amyloid β peptide (Aβ(1−40)) is thermodynamically soluble at physiological concentrations, *Biochemistry 42*, 10506−10513.
72. Hasegawa, K., Ono, K., Yamada, M., and Naiki, H. (2002) Kinetic modeling and determination of reaction constants of Alzheimer's β-amyloid fibril extension and dissociation using surface plasmon resonance, *Biochemistry 41*, 13489−13498.
73. LeVine, H., III. (1999) Quantification of β-sheet amyloid fibril structures with thioflavin T, *Methods Enzymol. 309*, 275−284.
74. Harper, J. D., Wong, S. S., Lieber, C. M., and Lansbury, P. T., Jr. (1999) Assembly of A beta amyloid protofibrils: an in vitro model for a possible early event in Alzheimer's disease, *Biochemistry 38*, 8972−8980.
75. Souillac, P. O., Uversky, V. N., Millett, I. S., Khurana, R., Doniach, S., and Fink, A. L. (2002) Elucidation of the molecular mechanism during the early events in immunoglobulin light chain amyloid fibrillation. Evidence for an off-pathway oligomer at acidic pH, *J. Biol. Chem. 277*, 12666−12679.
76. Baskakov, I. V., Legname, G., Baldwin, M. A., Prusiner, S. B., and Cohen, F. E. (2002) Pathway complexity of prion protein assembly into amyloid, *J. Biol. Chem. 277*, 21140−21148.
77. Sokolowski, F., Modler, A. J., Masuch, R., Zirwer, D., Baier, M., Lutsch, G., Moss, D. A., Gast, K., and Naumann, D. (2003) Formation of critical oligomers is a key event during conformational transition of recombinant syrian hamster prion protein, *J. Biol. Chem. 278*, 40481−40492.
78. Modler, A. J., Gast, K., Lutsch, G., and Damaschun, G. (2003) Assembly of amyloid protofibrils via critical oligomers—a novel pathway of amyloid formation, *J. Mol. Biol. 325*, 135−148.
79. Souillac, P. O., Uversky, V. N., Millett, I. S., Khurana, R., Doniach, S., and Fink, A. L. (2002) Effect of association state and conformational stability on the kinetics of immunoglobulin light chain amyloid fibril formation at physiological pH, *J. Biol. Chem. 277*, 12657−12665.
80. Stine, W. B., Jr., Dahlgren, K. N., Krafft, G. A., and LaDu, M. J. (2003) In vitro characterization of conditions for amyloid-beta peptide oligomerization and fibrillogenesis, *J. Biol. Chem. 278*, 11612−11622.
81. White, J. T., and Kelly, J. W. (2001) Support for the multigenic hypothesis of amyloidosis: the binding stoichiometry of retinol-binding protein, vitamin A, and thyroid hormone influences transthyretin amyloidogenicity in vitro, *Proc. Natl. Acad. Sci. U.S.A. 98*, 13019−13024.
82. Merlini, G., Ascari, E., Amboldi, N., Bellotti, V., Arbustini, E., Perfetti, V., Ferrari, M., Zorzoli, I., Marinone, M. G., Garini, P., Diegoli, M., Trizio, D., and Ballinari, D. (1995) Interaction of the anthracycline 4′-iodo-4′-deoxydoxorubicin with amyloid fibrils: inhibition of amyloidogenesis, *Proc. Natl. Acad. Sci. U.S.A. 92*, 2959−2963.
83. Lewis, W. D., Skinner, M., Simms, R. W., Jones, L. A., Cohen, A. S., and Jenkins, R. L. (1994) Orthotopic liver transplantation for familial amyloidotic polyneuropathy, *Clin. Transplant. 8*, 107−110.
84. Holmgren, G., Ericzon, B. G., Groth, C. G., Steen, L., Suhr, O., Andersen, O., Wallin, B. G., Seymour, A., Richardson, S., Hawkins, P. N., and Pepys, M. B. (1993) Clinical improvement and amyloid regression after liver transplantation in hereditary transthyretin amyloidosis, *Lancet 341*, 1113−1116.
85. Suhr, O. B., Ericzon, B. G., and Friman, S. (2002) Long-term follow-up of survival of liver transplant recipients with familial amyloid polyneuropathy (Portuguese type), *Liver Transpl. 8*, 787−794.
86. Miroy, G. J., Lai, Z., Lashuel, H. A., Peterson, S. A., Strang, C., and Kelly, J. W. (1996) Inhibiting transthyretin amyloid fibril formation via protein stabilization, *Proc. Natl. Acad. Sci. U.S.A. 93*, 15051−15056.
87. Peterson, S. A., Klabunde, T., Lashuel, H. A., Purkey, H., Sacchettini, J. C., and Kelly, J. W. (1998) Inhibiting transthyretin conformational changes that lead to amyloid fibril formation, *Proc. Natl. Acad. Sci. U.S.A. 95*, 12956−12960.
88. Klabunde, T., Petrassi, H. M., Oza, V. B., Raman, P., Kelly, J. W., and Sacchettini, J. C. (2000) Rational design of potent human transthyretin amyloid disease inhibitors, *Nat. Struct. Biol. 7*, 312−321.

BI049621L